Annu. Rev. Fluid Mech. 2002. 34:375–415
Copyright © 2002 by Annual Reviews. All rights reserved

FILAMENT-STRETCHING RHEOMETRY OF COMPLEX FLUIDS

Gareth H. McKinley[1] and Tamarapu Sridhar[2]
[1]*Department of Mechanical Engineering, Massachusetts Institute of Technology, Cambridge, Massachusetts 02139; e-mail: gareth@mit.edu*
[2]*Department of Chemical Engineering, Monash University, Melbourne, Victoria, Australia; e-mail: sridhar@eng.monash.edu.au*

Key Words transient extensional viscosity, polymer solution rheology, elongational flow

■ **Abstract** Filament-stretching rheometers are devices for measuring the extensional viscosity of moderately viscous non-Newtonian fluids such as polymer solutions. In these devices, a cylindrical liquid bridge is initially formed between two circular end-plates. The plates are then moved apart in a prescribed manner such that the fluid sample is subjected to a strong extensional deformation. Asymptotic analysis and numerical computation show that the resulting kinematics closely approximate those of an ideal homogeneous uniaxial elongation. The evolution in the tensile stress (measured mechanically) and the molecular conformation (measured optically) can be followed as functions of the rate of stretching and the total strain imposed. The resulting rheological measurements are a sensitive discriminant of molecularly based constitutive equations proposed for complex fluids. The dynamical response of the elongating filament is also coupled to the extensional rheology of the polymeric test fluid, and this can lead to complex viscoelastic-flow instabilities such as filament necking and rupture or elastic peeling from the rigid end-plates.

1. INTRODUCTION

Within the last decade, there has been an explosion of activity aimed at improving one's ability to measure and understand the response of polymer solutions to an extensional deformation. The importance of elongational or extensional flow of polymer fluids arises because several industrially important processes involve a predominantly extensional mode of deformation; examples include fiber spinning, film blowing, and extrusion of polymeric materials. For polymer solutions, extensional flows are also encountered in applications such as coatings, enhanced oil recovery, lubrication, turbulent drag reduction, and atomization. It is well known that the addition of a small amount of high molecular-weight polymer in solutions greatly increases the resistance to flow in extension. This property of

macromolecular fluids has been exploited in processes such as the prevention of the breakup of a jet of fluid emitting from a nozzle into droplets.

Even a cursory examination of current textbooks on rheology (e.g., Bird et al. 1987a, Tanner 2000) shows how much shear rheology dominates the science and how little is known comparatively regarding extensional deformation. Shear flows are weak in the sense that material elements in the fluid separate linearly with time, and vorticity ensures that the fluid microstructure is always rotated away from the principal axes of stretching. Extensional flows, on the other hand, are irrotational and extremely efficient at unraveling flexible macromolecules or orienting rigid molecules. As a result, one anticipates that if the flow field were to be maintained for a long enough time, all molecules would eventually be fully extended and aligned. As the force on the molecule depends both on the strain rate and elongation, extensional flows are expected to elicit, qualitatively and quantitatively, fluid responses different from simple shear flow. The extensional rheological properties of fluids are therefore expected to be a more critical test of the plethora of constitutive equations that have been proposed to describe the stress-deformation relationship of polymeric fluids.

2. FUNDAMENTAL DEFINITIONS

2.1. Kinematics of Extensional Flows

Consider the uniaxial elongation of a cylindrical specimen of initial diameter D_0 and length L_0, which is stretched in the axial direction z by an applied force F so that its radius decreases uniformly along the length. For a homogeneous shear-free flow, the kinematics are independent of spatial position. The flow is irrotational, and the velocity-gradient tensor is given by

$$\boldsymbol{\nabla v} = \frac{1}{2}\dot{\varepsilon}(t)\begin{pmatrix} -1 & 0 & 0 \\ 0 & -1 & 0 \\ 0 & 0 & 2 \end{pmatrix}, \tag{1}$$

where $\dot{\varepsilon}(t)$ is the extension rate. Positive values represent elongation, and negative values lead to biaxial stretching. If the extension rate is constant with time such that $\dot{\varepsilon}(t) = \dot{\varepsilon}_0$, then the flow is steady in both the Eulerian and Lagrangian senses. That is, at any position along the cylinder, the velocity gradient is constant with time, and furthermore, an element of fluid experiences a motion with constant stretch history. Then from conservation of volume and integration of the components of Equation 1, the length and diameter of the specimen at any time t vary from their initial values of L_0 and D_0, respectively, in the following way,

$$L(t) = L_0 \exp(\dot{\varepsilon}_0 t); \quad D(t) = D_0 \exp\left(-\frac{1}{2}\dot{\varepsilon}_0 t\right). \tag{2}$$

The natural-strain measure arising from such a deformation is the logarithmic or Hencky strain given by

$$\varepsilon = \dot{\varepsilon}_0 t = \ln(L(t)/L_0) = -2\ln(D(t)/D_0). \tag{3}$$

The total-stress tensor $\boldsymbol{\pi}$ for a fluid undergoing homogeneous uniaxial extensional flow is given by $\boldsymbol{\pi} = -p\boldsymbol{I} + \boldsymbol{\tau}$, where $-p\boldsymbol{I}$ is the isotropic pressure contribution and $\boldsymbol{\tau}$ is the extra-stress tensor, which must be determined from an appropriate constitutive equation. In the start-up of uniaxial extensional flow, the fluid is initially quiescent and the extra stress is identically zero. Then at times $t \geq 0$, the constant extension rate $\dot{\varepsilon}_0$ is imposed on the specimen, and the stresses grow in time as stretching progresses. The material function of interest is the transient extensional viscosity or tensile-stress growth coefficient $\eta_E^+(\dot{\varepsilon}_0, t)$, defined as

$$\eta_E^+(\dot{\varepsilon}_0, t) \equiv \frac{\tau_{zz} - \tau_{rr}}{\dot{\varepsilon}_0}. \tag{4}$$

As time increases and the deformation proceeds, the extensional- or tensile-stress growth coefficient may reach a steady-state value, which is termed the extensional or tensile viscosity,

$$\eta_E(\dot{\varepsilon}_0) = \lim_{t\to\infty} \left[\eta_E^+(\dot{\varepsilon}_0, t)\right]. \tag{5}$$

The extensional viscosity η_E is a material property of the fluid and is a function only of the extension rate (and temperature). For a Newtonian liquid with a constant shear viscosity, μ, substitution of the known kinematics into the Newtonian constitutive equation gives the result

$$\eta_E \equiv \frac{\tau_{zz} - \tau_{rr}}{\dot{\varepsilon}_0} = \frac{2\mu\dot{\varepsilon}_0 - (-\mu\dot{\varepsilon}_0)}{\dot{\varepsilon}_0} = 3\mu. \tag{6}$$

This result is often referred to as the Trouton viscosity, after Trouton (1906), who found that the extensional viscosity of a mixture of pitch and tar is independent of the rate-of-extension and is three times the shear viscosity of the mixture. For viscoelastic fluids in the limit of very low extension rates, simple fluid theory (Bird et al. 1987a) shows that the steady-state extensional viscosity also approaches three times the zero-shear viscosity.

The polymer stress provides a measure of the overall deformation of the polymer chain. In addition, it is useful to obtain a direct microstructural measure of the local orientation and conformational shape of the chain. Flow-induced birefringence can accurately and noninvasively provide such a measure. Birefringence arises from the anisotropy in the refractive-index tensor of the polymeric medium and results in a phase difference (or retardance) of polarized light traversing the sample. Details of the theoretical background and measurement techniques in various flow fields are available in the treatise by Fuller (1995). The principal elastic stress difference and

the birefringence $\Delta n'$ in extensional flow are related by the stress-optical rule (Larson 1988, Fuller 1995)

$$(\tau_{zz} - \tau_{rr}) \equiv \Delta\tau = \Delta n'/C, \tag{7}$$

where C is the stress-optic coefficient. It has been known for some time that this colinearity becomes invalid in strong extensional flows such as fiber spinning (Talbott & Goddard 1979), and the filament-stretching rheometers we describe below have also been developed to permit simultaneous and independent determination of the birefringence and polymeric tensile stress (Sridhar et al. 2000).

2.2 Historical Perspective

The continuing fascination of scientists with extensional flows has been well documented by Petrie (1979) in the only available treatise on extensional flows. The thread-forming ability of fluids has attracted the attention of researchers since the work of Trouton (1906). Measurements of the viscometric properties of polymeric fluids in simple shear flows are well established (Meissner 1985b), and a number of commercial rheometers are available for both melts and the more-mobile polymer solutions. The situation is far less satisfactory, however, when it comes to measuring the extensional material properties. Techniques have been developed for polymer melts, such as polyolefins, which are viscous enough that homogeneous sheets or rods of material can be prepared and elongated under conditions of either constant deformation rate or constant stress (Münstedt 1979, Meissner 1985a). As a result of the mobile nature of polymer solutions, it was thought to be impossible to grip the sample and make it stretch in a prescribed manner. The basic requirement for such measurements is the ability to impose a precise (preferably constant) deformation history on a fluid sample for a long enough period such that a constant stress is achieved.

Most of the techniques used for mobile liquids can be classified as either flow-through systems or stagnation-point devices. Among the former methods, fiber spinning seems to have been most widely used, as it represents the most promising method of providing a well-defined deformation field (Nitschman & Schrade 1948). Other free-surface techniques that have been used to measure the extensional viscosity of polymer solutions include the tubeless siphon, otherwise known as Fano flow (Astarita & Nicodemo 1970), and the triple-jet techniques (Oliver & Bragg 1974). Each configuration involves essentially the stretching of a fluid jet and measuring the resultant tensile force or stress required to sustain the extension. Fuller et al. (1987) have described an extensional rheometer that uses opposing nozzles immersed in the fluid. Sucking the fluid into the nozzles using a vacuum creates an extensional flow field in the small gap between the nozzles. Numerous variants of these techniques are available and are reviewed elsewhere (Gupta & Sridhar 1998). All of these approaches fail to achieve some of the kinematic requirements stated earlier (James & Walters 1993, Petrie 1995). The disappointing state of affairs as far as the measurements of the extensional properties of polymer solutions are concerned can be seen in the outcome of the M1 project.

This project attempted to compare the extensional viscosity measurements obtained by different techniques on a single fluid (Sridhar 1990). Suffice it to say, this exercise demonstrated the urgent need for a better method of measuring extensional properties.

Over the last decade, the filament-stretching rheometer has emerged as a new method of measuring extensional properties of mobile liquids (Matta & Tytus 1990, Sridhar et al. 1991, Tirtaatmadja & Sridhar 1993). The last few years have seen a rapid growth in the development and usage of this instrument. This review focuses on implementation and analysis of the filament-stretching technique and attempts to both demonstrate the considerable progress that has been made and discuss the significant new issues that have emerged and await clarification.

3. CONSTITUTIVE EQUATIONS FOR POLYMER SOLUTIONS

Non-Newtonian fluid mechanics is pedagogically different from Newtonian fluid mechanics, and polymeric fluids exhibit numerous characteristics that find no parallel in Newtonian fluids (Bird et al. 1987a). The viscoelastic nature of the materials means that the extra stress in a fluid element depends on the entire history of deformation experienced by that element. The stress can therefore be expressed as a functional of the velocity gradient, time, and other microstructural details. The numerous constitutive equations that have been developed for polymeric materials can be conveniently classified in many different ways depending on the user's perspective (for example see Bird et al. 1987b, Larson 1988). Space prohibits a detailed discussion of recent advances in these areas. Bird (1982) has reviewed the use of molecular models derived from kinetic theory. The monograph edited by Nguyen & Kausch (1999) also summarizes many recent developments in the study of dilute polymer solutions in extensional flows.

3.1. Kinetic Theories for Dilute Polymer Solutions

The development of a kinetic theory for polymers has been one of the outstanding intellectual achievements in rheology and allows a hierarchical description of the fluid microstructure that can be progressively and systematically reduced in dimensionality (coarse-grained). By correctly incorporating the molecular details, specific predictions (e.g., the scalings of the relaxation time and viscosity with molecular weight and concentration) can be obtained. For a detailed discussion of kinetic theory, the reader is referred to Bird et al. (1987b) and Appendix B (available as Supplemental Material: Follow the Supplemental Material link on the Annual Reviews homepage at http://www.annualreviews.org); however, the process can be summarized schematically, as shown in Figure 1. The enormous range of length scales (and timescales) evident in the figure permit a variety of modeling approaches. The simplest model is obtained by replacing all of the individual monomers by a single dumbbell; i.e., a massless linear (or nonlinear)

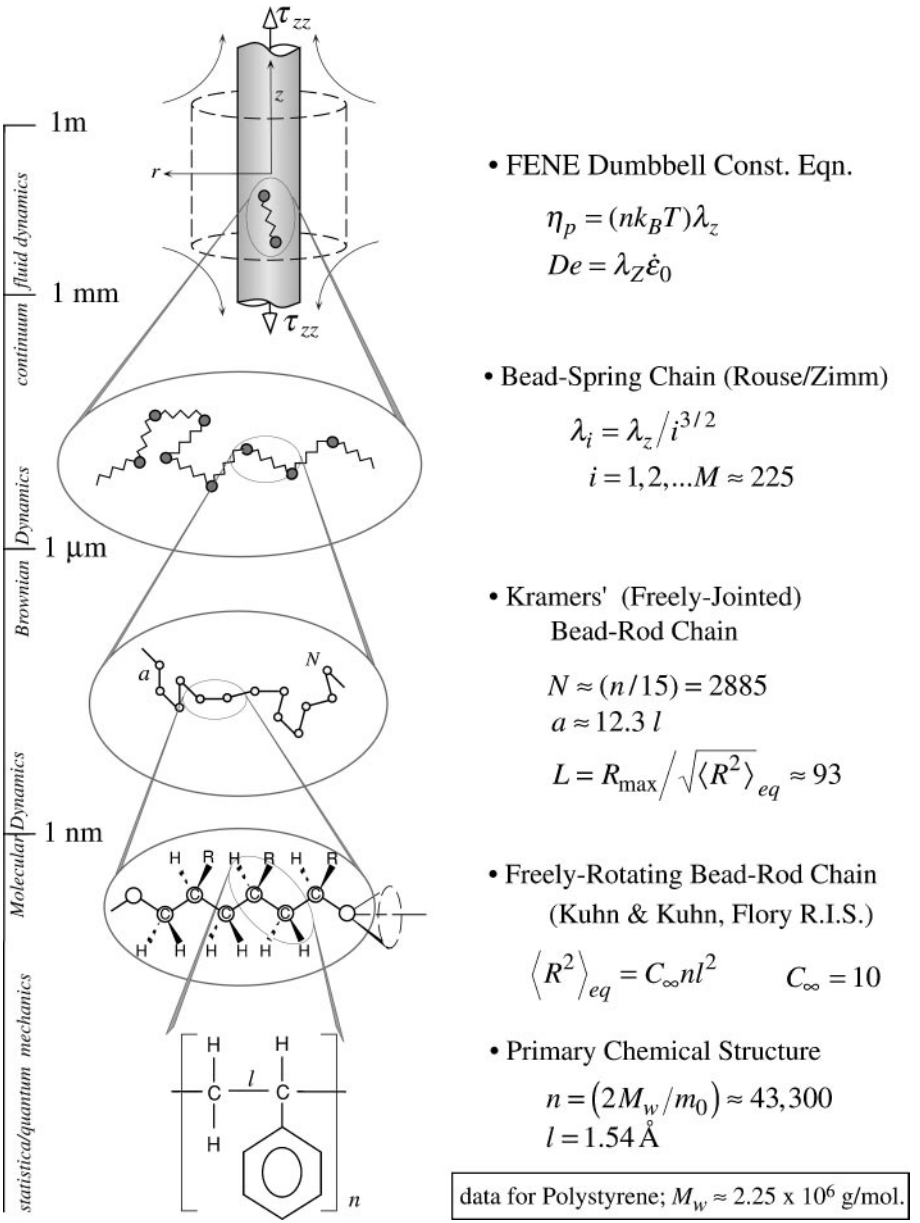

Figure 1 Progressive coarse graining in the hierarchy of microstructural modeling for dilute polymer solutions. The numerical values of the parameters shown are for a typical polystyrene (PS) molecule with a molecular weight of 2.25×10^6 g/mol.

spring with the mass of the chain evenly distributed between two point masses at either end of the spring. These "beads" are also the locus of all hydrodynamic interactions between the chain and the solvent. When external motion is imposed, the chain segments are subjected to hydrodynamic drag forces, an entropic spring force, Brownian motion, and appropriate constraints (for example see van den Brule 1993). For later reference, it is convenient to consider the response of such a prototypical viscoelastic constitutive equation in a homogeneous extensional flow. For clarity, we focus on the topmost or most "coarse-grained" level in Figure 1 (the dumbbell model) and consider the effects of finite extensibility in the spring and anisotropy in the drag acting on the chain. The conformation of the molecule can be presented by a single-evolution equation of the form

$$\frac{D\boldsymbol{A}}{Dt} - \{\nabla \boldsymbol{v}^T \cdot \boldsymbol{A} + \boldsymbol{A} \cdot \nabla \boldsymbol{v}\} = -\frac{1}{\lambda}[\boldsymbol{I} + \alpha(\boldsymbol{A} - \boldsymbol{I})] \cdot [f(tr\boldsymbol{A})\boldsymbol{A} - \boldsymbol{I}], \qquad (8)$$

where the conformation tensor $\boldsymbol{A} \equiv \langle \boldsymbol{QQ} \rangle / Q_{eq}^2$ is the ensemble average of the dyadic product of the dumbbell connector vector scaled with the equilibrium size of the freely jointed chain, $Q_{eq}^2 = Nb^{2/3}$. The single relaxation time of the chain is denoted by λ, α is a measure of the anisotropy in the drag acting on the dumbbell as it orients and elongates, and $f(tr\boldsymbol{A})$ is the nonlinearity of the spring.

From the conformation tensor, the total deviatoric stress arising from the solvent and the presence of the deformed dumbbells can be found to be

$$\boldsymbol{\tau} = \boldsymbol{\tau}_s + \boldsymbol{\tau}_p = \eta_s \dot{\gamma} + \nu k_B T[f(trA)A - I], \qquad (9)$$

where ν is the number density of polymer chains, k_B is Boltzmann's constant, and T is the absolute temperature. When $\alpha = 0$ and $f(tr\boldsymbol{A}) = [1 - tr\boldsymbol{A}/3N]^{-1}$, Equations 8 and 9 reduce to the FENE-P (finitely extensible nonlinear elastic) model, while $\alpha \neq 0$, $f(tr\boldsymbol{A}) = 1$ corresponds to the Giesekus model. In the limit $\alpha = 0$ and $f(tr\boldsymbol{A}) = 1$, the model becomes the Hookean dumbbell model or, equivalently, the Oldroyd-B equation of continuum mechanics (Bird et al. 1987a,b).

In an irrotational flow with specified kinematics (Equation 1), the differential equations for the evolution in the microstructural deformation become particularly simple to solve. Combining Equations 1, 8, and 9 leads to the following expression for the transient extensional viscosity of the Hookean dumbbell model,

$$\eta_E^+(\dot{\varepsilon}_0, t) = 3\eta_s + \frac{2\nu k_B T\lambda}{(1 - 2\lambda\dot{\varepsilon}_0)}[1 - \exp(-(1 - 2\lambda\dot{\varepsilon}_0)t/\lambda)]$$
$$+ \frac{\nu k_B T\lambda}{(1 + \lambda\dot{\varepsilon}_0)}[1 - \exp(-(1 + \lambda\dot{\varepsilon}_0)t/\lambda)]. \qquad (10)$$

The dimensionless product in Equation 10 is the Deborah number, $De = \lambda\dot{\varepsilon}_0$. For $|De| \ll 1$, Equation 10 reduces to the prediction of linear viscoelasticity with $\eta_E \equiv 3\eta_0 = 3(\eta_s + \nu k_B T\lambda)$ at steady state. For values $-1 < De < 0.5$, Equation 10 predicts the extensional viscosity approaches a steady-state value that is $O(De)$

above the linear viscoelastic limit; however, for $De \geq 0.5$, the extensional viscosity grows without bound, corresponding to a "coil-stretch transition" at a critical value of the Deborah number, as first described by de Gennes (1974). This transition has since been confirmed in numerous experiments, perhaps most unambiguously in the single-molecule imaging results of Chu and co-workers (Perkins et al. 1997, Smith & Chu 1998).

3.2. Constitutive Models for Entangled Polymeric Fluids

Constitutive equations for polymer melts and entangled solutions have been significantly influenced by the concept of reptation (Doi & Edwards 1986), which prescribes that in entangled systems the chain motion in the lateral direction is impeded by entanglement constraints. The chain changes its conformation by curvilinear diffusion (reptation) in the longitudinal direction within a confining tube. Numerous reviews of recent developments are available (for example see Watanabe 1999, Leal & Oberhauser 2000). In entangled solutions of linear macromolecules, there are two dominant timescales (and their associated spectra), the disengagement time $\lambda_d \sim Z^3\lambda_e$ for curvilinear diffusion (reptation) of the chain inside a tube of constraints and the Rouse time $\lambda_R \sim Z^2\lambda_e$. Here, the reference timescale denoted by λ_e is the Rouse time for a single entangled segment of the chain. The quantity $Z = M_w/M_e$ is the ratio of the molecular weight of the chain to the molecular weight between entanglements and is a measure of the average number of entanglements per chain. It is worth noting that simple differential approximations to the full integral formulations of typical reptation models (for example see Mead et al. 1998) can be written in forms very similar to that indicated in Section 3.1, with the following important differences: (*a*) The polymeric stress arises from evolution in both the orientation of the confining tube and the magnitude of the stretch of the polymer chain within the tube, and consequently, (*b*) two coupled evolution equations arise with time constants that characterize the orientational dynamics of the tube (the disengagement timescale, λ_d) and the separate relaxation of the stretched polymer chain within the tube (the Rouse time, λ_R). We return briefly to the predicted extensional rheology of such models in Section 6.4.

4. THE FILAMENT STRETCHING RHEOMETER

4.1. Device Design and Operating Conditions

A basic schematic diagram of a filament-stretching device is shown in Figure 2. The drive train accommodates the end plates, and the electronic control system imposes a predetermined velocity profile on one or both of the end plates. The principal time-resolved measurements required are the force $F(t)$ on one of the end plates and the filament diameter at the midplane. Modified analytical balances have been used to measure the force; however, cantilever force transducers with a resolution

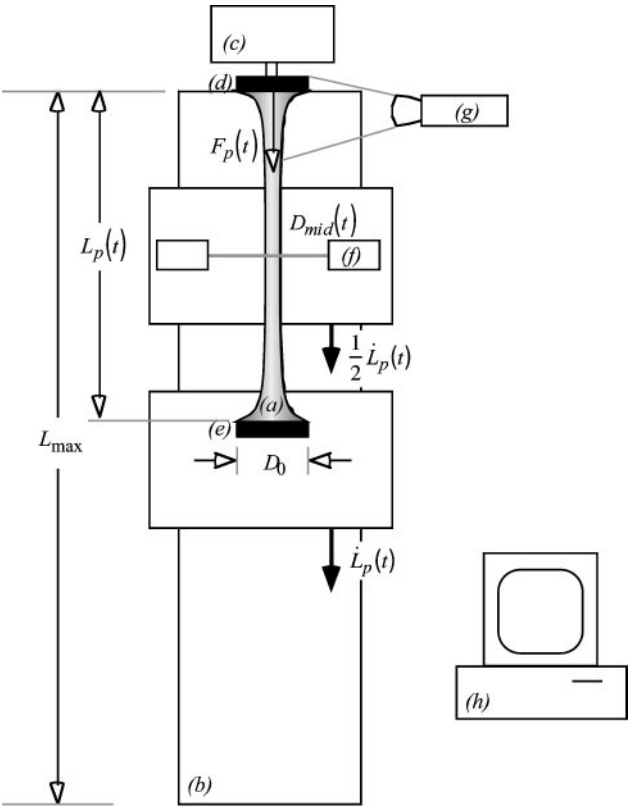

Figure 2 Schematic diagram of a filament-stretching instrument showing the principal components of the device (Reproduced from Anna et al. 2001).

of O(10^{-4} g) and response times of O(10^{-3} s) are especially suitable for this application and are commercially available. The filament diameter can be measured by using devices such as laser micrometers or wire gauges or by analyzing video images of the extending filament. The former provides better temporal resolution at a fixed point, which we denote henceforth as $D_{mid}(t)$, whereas the latter yields the entire diameter profile $D(z, t)$ albeit with somewhat reduced accuracy.

The geometric dimensions and motor capacity of the motion-control system determine the range of experimental parameters accessible in a given filament-stretching device. Figure 3 depicts the generic operating space for a filament-stretching device, where endplate velocity is plotted as a function of the endplate position. The maximum length of the drive, $L_{\max}$, and maximum velocity, $V_{\max}$, achievable by the motors form the bounds of the operating space. An ideal uniaxial extensional flow, described by Equation 2, is represented as a straight line on this phase diagram, with a slope equal to the imposed strain rate. It is clear from the

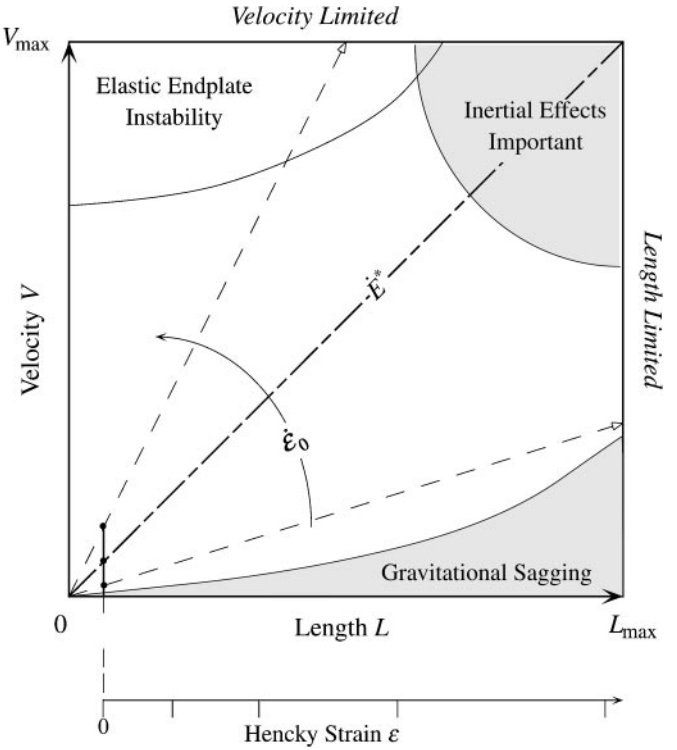

Figure 3 Sketch of the typical operating space of a filament-stretching rheometer and the known instabilities that constrain operation.

diagram that a given experiment will be limited by either the total travel available to the motor plates or by the maximum velocity the motors can sustain. An important characteristic for any such device is the characteristic strain rate $\dot{E}^* = V_{max}/L_{max}$ at which both the motor limit and the maximum stage length are simultaneously attained. The mechanical and geometric parameters characterizing a number of current filament-stretching devices have been tabulated by Anna et al. (2001). The operating space accessible with a given fluid can also be further constrained by instabilities associated with gravitational sagging, capillarity, and/or elasticity. The location of these stability boundaries depends on the material properties of the fluid and are discussed further in Section 4.3.

The fluid sample is initially constrained between two coaxial circular plates to form a liquid bridge of aspect ratio $\Lambda_0 \equiv L_0/R_0$ and is subsequently elongated by the motion of either the upper or lower plates. A typical sequence of images for a dilute polymer solution undergoing stretching is shown in Figure 4. Note that over a large portion of the filament length, the diameter is axially

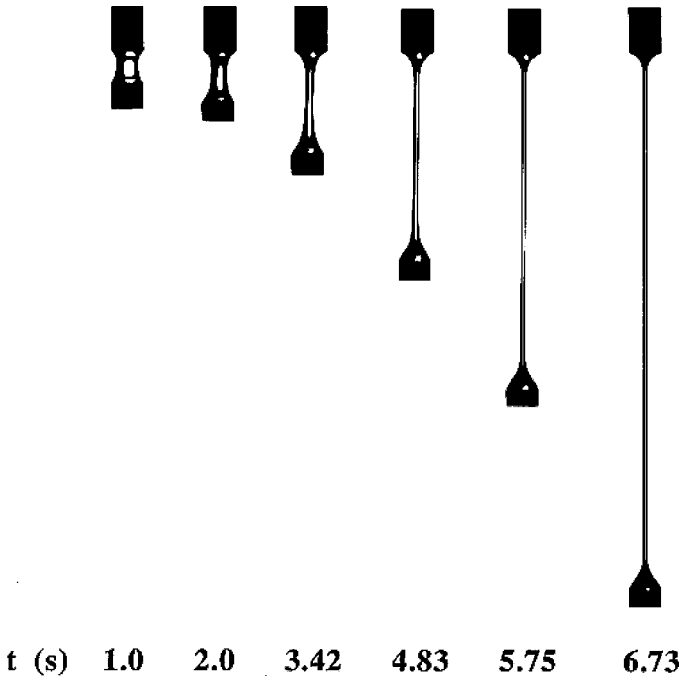

Figure 4 Photographic images of a viscoelastic fluid filament (0.31wt% polyisobutylene in polybutene) during exponential elongation at $\dot{\varepsilon}_0 = 0.76\text{s}^{-1}$; the plate dimensions are $D_0 = 0.303$ cm $L_0 = 0.18$ cm (Reproduced from Sridhar et al. 1991).

uniform as desired for homogeneous elongation. However, the no-slip condition at the endplates does cause a deviation from uniformity. The consequences of this are examined in Section 4.5. For strongly strain-hardening materials, Hencky strains of up to $\varepsilon \approx 7$ [corresponding to a macroscopically imposed stretch of $L_{\max}/L_0 = \exp(7) \approx 1100$] can be achieved.

4.2. Filament Evolution During Elongation

The general evolution in the principal experimental observables in a filament-stretching rheometer [i.e., the midpoint radius $R_{mid}(t)$ and the axial force $F(t)$] typically exhibit three characteristic regimes: (*a*) filament elongation, (*b*) stress relaxation, and (*c*) filament breakup.

During elongation (regime *a*), the radius decreases exponentially. At short times (or early strains $\varepsilon \leq 1$), there is an initial, solvent-dominated peak in the force, followed by a steady decline due to the exponential decrease in the cross-sectional area of the filament. At an intermediate strain $\varepsilon \approx 3$, the force begins to increase again owing to the strain hardening in the tensile stress. Because the area is still decreasing exponentially, an increasing force indicates that the polymeric stress

must be increasing faster than $\exp(\varepsilon)$, in agreement with Equation 10 for $De \geq 1$. At very large strains ($\varepsilon \geq 5$), a second maximum in the force may be observed after the extensional stresses saturate and the extensional viscosity of the fluid reaches its steady-state value, $\eta_E(\dot{\varepsilon}_0)$.

Following cessation of stretching at a strain ε_1, a second regime (*b*) ensues in which the tensile stresses in the filament rapidly relax while the radius remains almost constant. This region is typically short, lasting only one or two fluid relaxation times (Yao et al. 1998). Measurements of stress relaxation have been performed under these conditions and are discussed in Section 6.2. As the elastic stresses decay, capillary pressure and gravitational stresses become increasingly important and filament breakup ensues (regime *c*). The force rapidly decays and the radius decreases in a self-similar manner. Entov et al. (1988, Basilevsky et al. 1990) have pioneered the development of a related device referred to as a filament microrheometer, which utilizes this visco-elasto-capillary self thinning (and ultimate breakup) of a fluid thread in regime *c* to extract constitutive parameters characterizing the extensional viscosity of complex fluids. A more detailed discussion of such self-thinning experiments is beyond the scope of this review, and the reader is referred to a short review published elsewhere (McKinley 2000).

An important experimental issue in both filament-stretching devices and filament microrheometers is the minimum force and radius that can be measured experimentally because this constrains the range of fluids that can be tested. Typical values are $R_{\min} \approx 5\,\mu$m and $F_{\min} \approx 1 - 10$ mg. From a practical standpoint, the latter limitation has prohibited filament-stretching experiments to date for fluids of viscosity $\eta_0 \leq 1$ Pa.s.

4.3. Force Balance

A force balance is required to relate the measured force on the endplate to the stress difference in the fluid and hence the extensional viscosity. The effects of gravity, inertia, and surface tension need to be incorporated correctly, and an additional complicating factor is that the principal experimental measurables [i.e., the force $F(t)$ and midfilament diameter $D_{mid}(t)$] are measured at two separate axial locations. Some care is thus required in developing an appropriate force balance for the device. The most comprehensive treatment of the force balance is due to Szabo (1997) and is summarized below. The axial component of the linear-momentum equation is radially averaged and then integrated over the upper half of the filament from $0 \leq z \leq L/2$ to arrive at an equation for the mean stress in the filament:

$$\langle \tau_{zz} - \tau_{rr} \rangle + \frac{1}{2}\langle \tau_{rr} - \tau_{\theta\theta} \rangle + \frac{1}{2}\langle r\,\tau_{rz} \rangle' = \frac{F}{\pi R^2} - \frac{\rho g V_0}{2\pi R^2} - \frac{\sigma}{R}(1 + RR'') - \rho\left[\frac{1}{R^2}\frac{d^2}{dt^2}\int_0^{L/2} zR^2\,dz - \frac{R\ddot{R}}{4}\right]. \quad (11)$$

Here, $F(t)$ is the force on the upper endplate, $V_0/2$ is the volume of fluid in the upper half of the filament, and σ is the surface tension. The angular brackets indicate

average values over the filament cross section, and primes and overdots indicate differentiation with respect to axial position and time, respectively. The final terms on the right-hand side are the contributions due to gravity, surface tension and inertia, respectively. Experiments (Spiegelberg et al. 1996) and numerical simulations (Yao et al. 1998) show that, for judicious choices of the aspect ratio Λ_0, the flow field at the axial midplane is, to a good approximation, purely extensional. Assuming the fluid sample is initially at rest [such that $\tau_{ii}(t=0)=0$], then under such conditions the second and third terms on the left-hand side of Equation 11 are negligible. In addition, under conditions of constant strain rate, the last term on the right-hand side of Equation 11 is also negligible, and the extensional viscosity can be found from

$$\eta_E^+ \dot{\varepsilon}_0 \equiv \langle \tau_{zz} - \tau_{rr} \rangle = \frac{F}{\pi R^2} - \frac{\rho g V_0}{2\pi R^2} - \frac{\sigma}{R}(1 + RR'') - \rho \left[\frac{1}{R^2} \frac{d^2}{dt^2} \int_0^{L/2} zR^2 \, dz \right]. \quad (12)$$

There are several variants of this final force balance, depending on which plate is moved and at which plate the force transducer is located. In the original version introduced by Sridhar et al. (1991), the force on the stationary upper plate was measured, whereas an exponentially increasing velocity was imposed on the lower plate. As a result, the length of the filament followed Equation 2. However, axial nonuniformity of the filament resulted in the midpoint filament diameter deviating from Equation 3. Tirtaatmadja & Sridhar (1993) compensated for this effect by allowing both endplates to move in such a manner that the midfilament diameter followed Equation 2 (see Section 4.4 below), and the force was measured on the moving top plate. Spiegelberg et al. (1996) and Solomon & Muller (1996) measured the force on the stationary lower plate. Szabo (1997) gives appropriate versions of Equation 12 for each of these configurations. For most polymer solutions tested in filament-stretching devices to date, inertial effects are very small and the final term in Equation 12 is also typically neglected.

4.4. Dimensionless Groups

The most important dimensionless groups characterizing the filament-stretching rheometer are the Hencky strain, ε, characterizing the extent of deformation, and the Deborah number, $De \equiv \lambda \dot{\varepsilon}_0$, which characterizes the rate of stretching. In some publications, the dimensionless product $\lambda \dot{\varepsilon}_0$ is referred to as a Weissenberg number; however, we view this as inconsistent with conventional usage (Bird et al. 1987a) and as more relevant to the description of the initial radial shearing flow between the coaxial disks as they are separated. A standard lubrication analysis in the limit $\Lambda_0 = L_0/R_0 \ll 1$ (Spiegelberg et al. 1996) gives the magnitude of the radial deformation rate as $\dot{\gamma} = \partial v_r/\partial z \sim \dot{\varepsilon}_0/\Lambda_0^2$, and hence, the Weissenberg number is more properly defined as $Wi = \lambda\dot{\gamma} = De/\Lambda_0^2$. Several computational analyses (Yao & McKinley 1998, 2000; O. Harlen, unpublished results) have

shown that a homogenous uniaxial extensional flow can most readily be generated using initial aspect ratios $\Lambda_0 \approx 1$, and hence, these two dimensionless measures of the rate of deformation are frequently equivalent.

It is also instructive to nondimensionalize Equation 12 and examine the relative magnitudes of each term in comparison with the viscoelastic stress. If a viscous scale $\eta_0\dot{\varepsilon}_0$ is chosen for the stress, then three dimensionless groups arise from this equation. These groups can be expressed in terms of the familiar Reynolds number $Re = \rho\dot{\varepsilon}_0 R_0^2/\eta_0$, the Bond number $Bo = (\rho g R_0^2/\sigma)(L_0/R_0)$, and the capillary number $Ca \equiv \eta_0\dot{\varepsilon}_0 R_0/\sigma$.

For experiments with mobile fluids in a 1 g environment, gravitational "sagging" is a particularly important issue in filament-stretching devices. As the experiment progresses, there is a weak axial flow along the column so that more than 50% of the fluid volume lies below the midplane where the midpoint radius $R_{mid}(t)$ is measured. This can lead to significant systematic errors and even a change in sign in the Trouton ratio determined from Equation 12. Anna et al. (2001) present a detailed discussion of this gravitational sagging and show that it becomes significant when capillary forces in the neck near the axial midplane are no longer able to overcome the axial body force. This corresponds to a point at which $Bo/Ca \sim O(1)$ and leads to a critical strain rate $\dot{\varepsilon}_{sag} \approx \rho g L_0/\eta_0$, which must be exceeded in order to minimize the role of gravitational sagging. Because the viscosity and the relaxation time of a polymeric fluid both depend on the concentration and molecular weight (Bird et al. 1987a,b, Larson 1998), this limits the range of Deborah numbers that can be explored.

For dilute solutions described by the Zimm theory, this range of Deborah numbers can be expressed as

$$De \geq De_{sag}^{(dilute)} \equiv \frac{\lambda_Z \rho g L_0}{\eta_0} = \frac{2.369[\eta]M_w \rho g L_0}{(N_A k_B T)(1 + [\eta]c\cdots)}, \tag{13}$$

where N_A is Avagadro's number and M_w is the molecular weight of the chain (Anna et al. 2001). The intrinsic viscosity or "limiting viscosity number" $[\eta]$ can also be expressed in terms of the molecular weight using the Mark-Houwink relationship $[\eta] = K'(M_w)^a$ in which K' and a are tabulated constants for a particular polymer-solvent pair (Brandrup & Immergut 1997).

For entangled polymer solutions and melts, the (typically) very large viscosities lead to very low critical values of $\dot{\varepsilon}_{sag}$, and gravitational effects are, at first glance, less of an issue. However, the relaxation time also increases concomitantly with molecular weight, and hence, the range of Deborah numbers accessible without significant gravitational effects is still constrained. From reptation theory, the zero-shear viscosity and relaxation time for a well-entangled material are interconnected by $\eta_0 \approx G_N^0 \lambda_d$, where $\lambda_d \sim (M_w/M_e)^{3.4}$ is the reptation time and G_N^0 is the plateau modulus (Doi & Edwards 1986). For an entangled polymeric system of concentration c, the rubbery plateau modulus is independent of the molecular weight of the chain but can be expressed in terms of M_e, the molecular weight between entanglements (Doi & Edwards 1986). The range of Deborah numbers

achievable in a filament stretching device is thus

$$De \geq De_{sag}^{(conc)} \equiv \frac{\lambda_d \rho g L_0}{\left(G_N^0 \lambda_d\right)} = \frac{5}{4}\left(\frac{\rho}{c}\right)^2 \frac{M_e g L_0}{N_A k_B T}. \tag{14}$$

For a polystyrene melt ($M_e \approx 13{,}300$ g/mol) in a filament-stretching device of scale $L_0 = 1.5$ mm, we thus find $De_{sag} \approx 0.024$. For entangled polymer solutions, the plateau modulus decreases with dilution from the melt according to Equation 14, and as a result, De_{sag} increases rapidly. For a 10 wt% solution, $De_{sag} \approx 2.4$. This can severely constrain the lower range of Deborah numbers accessible in polymer melts.

4.5. Velocity Compensation

In an ideal extensional flow, the filament radius remains uniform along the length of the elongating fluid cylinder. However, when an exponentially increasing length is programmed into a filament-stretching device, analysis of image profiles such as those in Figure 4 do show some small but systematic deviations from such an expectation, especially near the filament ends. These deviations arise from the fixed endplates and cause the actual deformation history experienced by the fluid elements near the axial midplane to be different from that imposed at the rheometer endplates.

The magnitude and form of this discrepancy depend intimately on the rheological properties of the fluid filament (Solomon & Muller 1996). A typical result from an experiment in which the filament length follows Equation 2 is shown in Figure 5. Such an experiment has been termed a type I experiment (Kolte et al. 1997), and henceforth we use their nomenclature. It is evident that the diameter of the filament does not follow Equation 2, and the instantaneous deformation rate experienced by the fluid element at the axial midplane of the filament is given by

$$\dot{\varepsilon}_{mid}(t) = -\frac{2}{D_{mid}(t)} \frac{d D_{mid}(t)}{dt}. \tag{15}$$

Because the ends are pinned at the disk radius, the middle regions of the elongating liquid bridge must flow radially inward at a faster rate to conserve volume. This implies that the strain rate computed from analysis of midplane diameter data (Equation 15) and the value derived from filament length data (Equation 2) are not identical. A lubrication analysis (see Section 5.2 below) shows that the radial strain rate is, in fact, initially 50% larger than the axial strain rate. At longer times and larger aspect ratios, the difference becomes much smaller. The Hencky strain accumulated by the midpoint element at any time t can be found by direct integration of Equation 15 to give

$$\varepsilon_{mid} = \int_0^t \dot{\varepsilon}_{mid}\, dt' = 2 \ln(D_0 / D_{mid}(t)), \tag{16}$$

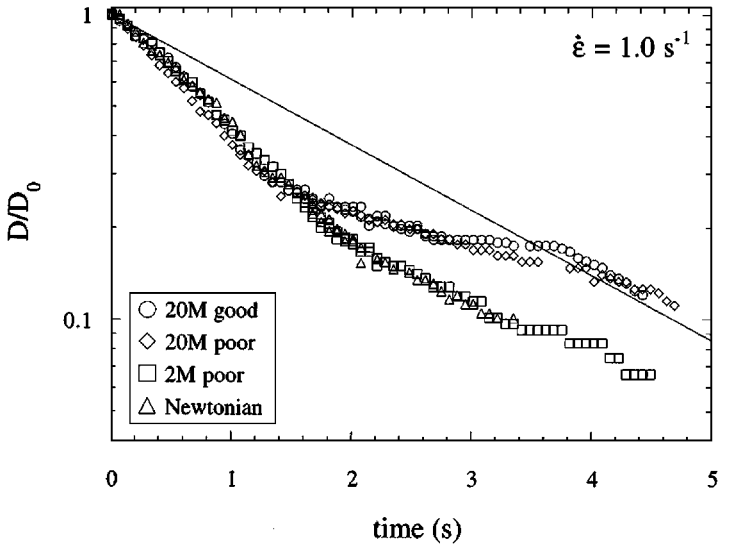

Figure 5 Radius profiles for a dilute polystyrene solution during filament stretching using a type I and a type II experimental protocol (see text for details) (Reproduced from Solomon & Muller 1996).

where $D_0 = 2R_0$ is the diameter of the endplates. In a type II experiment, the temporally inhomogeneous strain rate based on the midfilament diameter rather than the length is used to compute the viscosity. Kolte et al. (1997) discuss the errors in such experiments and conclude that a type III experiment in which the length profile $L(t)$ is continuously adjusted to ensure that the diameter profile follows Equation 2 is almost equivalent to an ideal uniaxial deformation. In other words, this ensures that the fluid elements near the midplane experience a motion with constant stretch history. Tirtaatmadja & Sridhar (1993) and Spiegelberg et al. (1996) achieved such a result empirically by using velocity profiles that are sums of two exponential functions: For a strongly strain-hardening material, this ensures that the diameter, to a good approximation, follows Equation 2. This trial and error procedure can be replaced by a more systematic velocity compensation or "master plot" technique (Orr & Sridhar 1999, Anna et al. 1999) that uses the following relationship relating the filament length and diameter,

$$(L(t)/L_0) = (D_0/D(t))^{p(t)}. \tag{17}$$

This relationship can be derived from a slender-body theory for the elongating filament (see Section 5.2 below), and the time-varying index spans the range $0 \leq p(t) \leq 2$. Ideal elongation of a cylinder gives $p = 2$, and the lubrication theory (as noted in Section 5.2 below) gives $p = 4/3$ at short times.

In general, for viscoelastic fluids, the function $p(t)$ can be evaluated by conducting a type I experiment and generating a kinematic master plot of the endplate

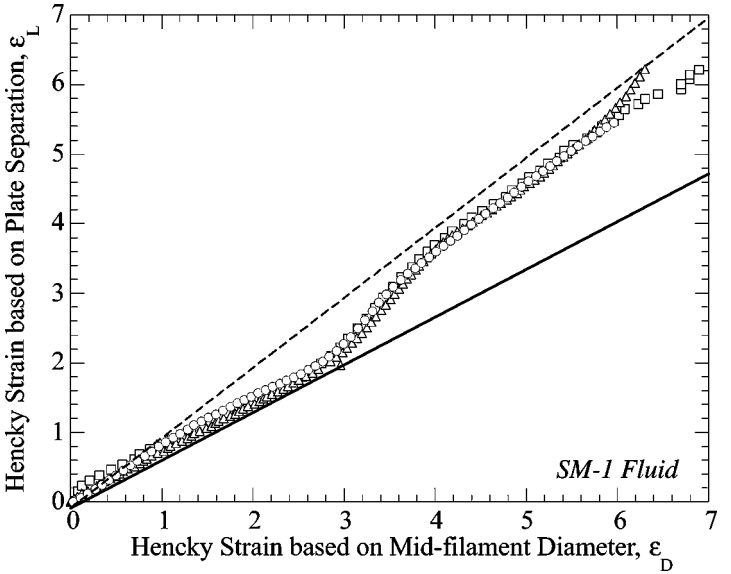

Figure 6 A kinematic master plot showing the evolution in the imposed axial strain ε_L and the resulting strain ε_{mid} experienced by fluid elements at the midplane of the elongating filament (Reproduced from Anna et al. 2001). The dashed and solid lines indicate the ideal and lubrication solutions, respectively.

strain $\varepsilon_L = \ln(L(t)/L_0)$ as a function of the effective or actual midplane strain ε_{mid} given by Equation 16. A typical master plot is shown in Figure 6. For viscous Newtonian fluids in the absence of surface tension, the mapping function $p(t)$ then allows the direct calculation of the required profile $L(t)$ for any desired $D(t)$. The incorporation of constitutive nonlinearities or capillarity mean that this inversion using $p(t)$ is not unique. However, numerical computations (McKinley et al. 2001) show that an "open-loop" control based on successive substitution [in which the i-th realization $p^{[i]}(t)$ is used to generate the next approximation $L^{[i+1]}(t)$ to the desired profile] rapidly and robustly converges. Anna et al. (1999) also discuss the implementation of a real-time "closed" control scheme to achieve constant strain rates; however, such approaches have to date proved dynamically unstable.

Using such techniques to achieve constant effective strain rates at the midplane of the filament allows reliable measurements for the transient uniaxial extensional viscosity function to be systematically obtained. A representative result from a recent interlaboratory comparison of filament-stretching devices using a polystyrene-based elastic test fluid is shown in Figure 7. The data show a rapid stress growth at zero time and a plateau at the expected initial Trouton ratio of $3\eta_s/\eta_0$. When the total strain exceeds $\varepsilon \sim 2$, the polymer molecules uncoil and the polymeric stress grows rapidly before reaching a steady state at a strain $\varepsilon \approx 6$. Figure 7 demonstrates excellent agreement between laboratories and is in marked contrast to the disappointing results of the M1 study (James & Walters 1993).

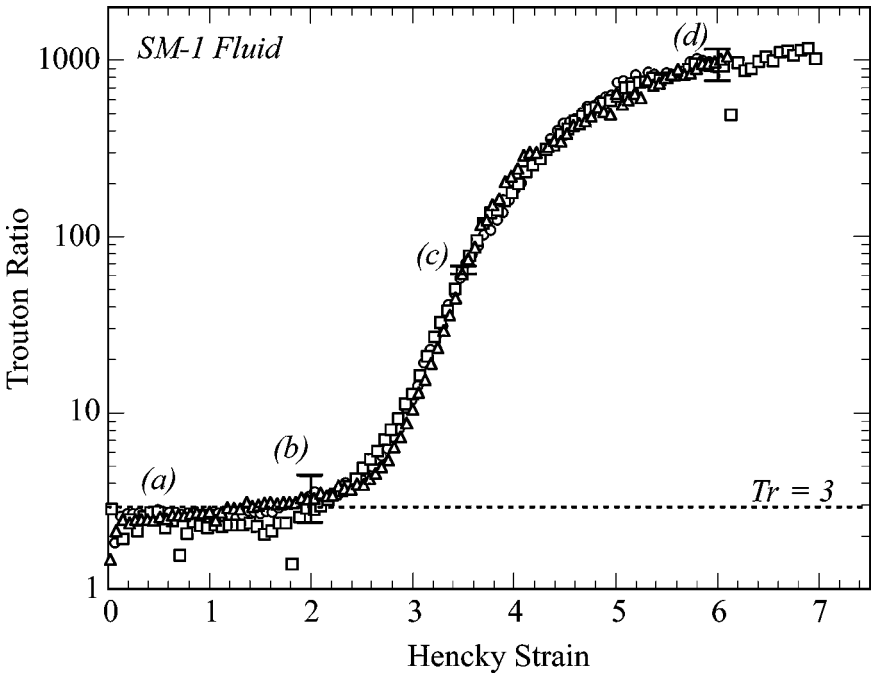

Figure 7 The transient extensional viscosity of a dilute (0.05 wt%) solution of monodisperse polystyrene ($M_w = 2 \times 10^6$ g/mol) (Reproduced from Anna et al. 2001).

The constitutive implications of such measurements of the transient extensional viscosity are discussed in detail in Section 6.

5. DYNAMICS OF FILAMENT-STRETCHING DEVICES: COMPUTATIONAL RHEOMETRY

Numerical analyses of the fluid motion in filament-stretching devices have been invaluable in confirming that a true homogeneous uniaxial elongation can indeed be achieved. Computational rheometry allows one to systematically vary the magnitude of dimensionless parameters, such as the initial aspect ratio, the Bond number, capillary number, or Reynolds number, and then compare the rheological output of the device (computed using Equation 12) with the result expected in ideal homogeneous uniaxial elongation. Similar computational-rheometry studies of the opposed-jet extensional rheometer (Fuller et al. 1987) have shown that although this device can be used to index the relative response of one complex fluid to another it cannot quantitatively determine the true Trouton ratio of a material, even in the limiting case of creeping flow of a Newtonian fluid (Dontula et al. 1997).

By contrast, numerous recent computational studies have shown that with judicious choice of experimental parameters (such as the initial aspect ratio) filament-stretching devices can accurately determine the full transient extensional viscosity function $\eta_E^+(\dot{\varepsilon}_0, t)$. The most important difference between filament-stretching devices and other extensional rheometers is that the full Lagrangian history of the material element located at the axial midplane of the device is followed in time. By contrast, spinline rheometers and other open-flow devices may be steady in an Eulerian sense, but fluid elements experience a complex and unsteady deformation history as they flow through the measuring volume.

5.1. Numerical Implementation

Numerical analysis of the dynamics in a filament-stretching device requires time-dependent simulations of a free-surface motion of a viscoelastic fluid. Such computations were impractical until just a few years ago. However, it is beyond the scope of this review to discuss details of recent developments in the numerical algorithms involved; the reader is instead referred to a recent survey by Baaijens (1998). The sole simplifying features of the present problem are that (*a*) the initial conditions of the quiescent liquid bridge are well defined and that (*b*) the initial non-Newtonian stress is zero. The first attempts to simulate such a motion were made by Shipman et al. (1991); however, only small Hencky strains ($\varepsilon \leq 1$) could be attained with computational resources at the time. More recently, simulations to large Hencky strains have been achieved using adaptive Eulerian finite-element methods for differential viscoelastic constitutive equations (Sizaire & Legat 1997; Sizaire et al. 1999; Yao et al. 1998, 2000) and a Lagrangian finite-element approach for integral constitutive equations (Kolte et al. 1997, Hassager et al. 1998). Results have also been obtained using a boundary-element method (Gaudet & McKinley 1998) and a hybrid Brownian-dynamics/finite-element (CONNFESSITT) algorithm (J. Cormenzana, A. di Cecca, J. Ramirez, & M. Laso, submitted).

5.2. Results From Numerical Analysis of Filament-Stretching Rheometers

LUBRICATION THEORY The evolution in the filament profiles predicted for three different constitutive models (N, Newtonian; G, Giesekus; O, Oldroyd-B) are shown in Figure 8 over a range of strains. At low Hencky strains, all three fluid columns look very similar. For viscous fluids, a lubrication analysis can be used to analyze the kinematics even though the aspect ratio $\Lambda(t)$ is not necessarily small. As a result of the no-slip boundary conditions that apply across the surface of the endplates, a shearing motion, which is essentially a "reversed squeeze flow," is induced (Spiegelberg et al. 1996). The axial velocity profile in the thread becomes cubic rather than linear in *z*, as required by the kinematics in Equation 1. If the imposed axial deformation rate is here denoted $\dot{E}$ [such that $L(t) = L_0 \exp(\dot{E}t)$], then the deformation rate at the midplane as measured by a laser micrometer is $\dot{\varepsilon}_{mid} = 3\dot{E}/2$ (Spiegelberg et al. 1996) and the endplate position and midplane

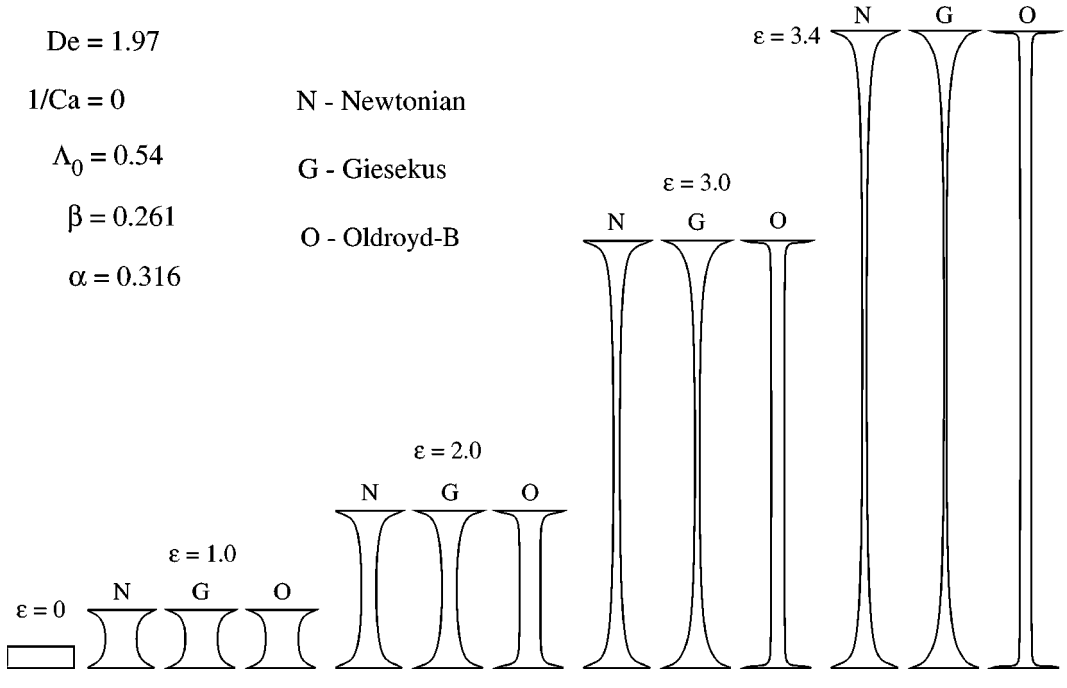

Figure 8 Axial profiles for transient uniaxial elongation of fluid filaments modeled by the Newtonian (N), Oldroyd-B (O), and Giesekus (G) constitutive models. The same viscometric properties and stretch rate are used in each simulation (corresponding to $De = 1.97$ for the viscoelastic fluids) (Reproduced from Yao et al. 1998).

radius are related by the following expression:

$$(L(t)/L_0) = (R_0/R_{mid}(t))^{4/3} = \exp(\dot{E}t). \tag{18}$$

The first equality gives the equation of the lubrication profile on the kinematic master curve, as discussed in Section 4.5. The net force exerted on the endplate at $t = 0^+$ also depends on the initial aspect ratio of the filament and serves as an indication of the nonideality of the flow at the start of the experiment. Numerical computations (Yao et al. 1998) show that for viscous filaments the kinematics remain in this lubrication regime until $\varepsilon \approx 1$.

SLENDER-BODY THEORY At large strains ($\varepsilon \geq 2$), experimental observations such as those in Figure 4 show that the elongating fluid columns become increasingly slender and axially uniform. The development of an appropriate self-consistent equation set for slender viscoelastic fluid threads is described by Schultz (1982), and a Lagrangian formulation that is particularly convenient for integration of typical nonlinear differential viscoelastic constitutive equations is detailed by Renardy (1994). In the development of these equations, the kinematics of the thread are taken to be one dimensional and of the general form

$$v_z = f(z); \qquad v_\theta = 0; \qquad v_r = -\frac{1}{2}rf'(z), \tag{19}$$

which automatically satisfies continuity and reduces the problem to the determination of $f(z)$ plus (in the case of non-Newtonian filaments) the integration of a set of coupled nonlinear ordinary differential equations for the unknown components of the stress tensor (see Phan-Thien & Tanner 1984). The ideal homogeneous solution corresponds to $f(z) \equiv \dot{\varepsilon}_0 z$.

A consequence of Equation 19 is that the velocity-gradient tensor becomes increasingly one dimensional and extension dominated as the filament elongates. If the axial velocity is $O(\dot{\varepsilon}_0 L)$, then the shearing-velocity gradient ($\partial v_r/\partial z$) arising from the last term in Equation 19 is only $O(\dot{\varepsilon}_0 R/L)$. For exponential stretching, $R \sim R_0 \exp(-\varepsilon/2)$ and $L \sim L_0 \exp(\varepsilon)$, and the transverse velocity gradients therefore decay very rapidly with strain. Contour plots of the deformation gradients determined from numerical simulations show that the radial variations are indeed negligible, except in small regions of axial extent $\Delta Z \sim R$ near either endplate (Sizaire & Legat 1997, Kolte et al. 1997, Yao & McKinley 1998). In these regions, two-dimensional shearing flows arise owing to the $O(1)$ combined effects of axial curvature and the no-slip boundary conditions on the endplates. Such effects cannot be captured in the one-dimensional kinematics of Equation 19, and this solution is best thought of as an "outer solution" for axial scales $z \sim L$, which must be matched to a local "inner solution" on scales $z \sim R$ near either endplate (Olagunju 1999). Despite this deficiency, numerical calculations show that the slender-filament equations provide a good approximation to the full equation set (Yao et al. 1998, Yildirim & Basaran 2001).

STRESS BOUNDARY LAYERS: THE ROLE OF INITIAL CONDITIONS One important outcome of full numerical simulations that cannot be readily captured by one-dimensional models has been the recognition that the choice of initial aspect ratio, $\Lambda_0 \equiv L_0/R_0$, is critical in ensuring that the flow generated in a filament-stretching device faithfully emulates the idealized uniaxial exponential kinematics desired for rheometry. Simulations confirm that the relative strength of the shearing components compared to the extensional terms in the kinematics of the initial squeeze flow are $O(\Lambda_0^{-1})$. The shearing deformation is greatest near the free surface, and this leads to radial variations in the initial microstructural deformation accumulated by fluid elements (Yao et al. 1998, Sizaire et al. 1999). In the supplementary material, we show that, for $De > 0.5$, initial radial nonhomogeneities in the initial polymer configuration $A_{zz}^{(0)}(r)$ never decay but are simply advected forward in time (cf. Equation B.8). Because the magnitude of the stretch is directly connected to the polymeric stress τ_{zz}, the evolution in this radial gradient leads to the development of sharp boundary layers in the axial stress near the free surface of the filament (Yao et al. 1998, Sizaire et al. 1999). Experimental measurements of integrated quantities, such as the birefringence or the total axial force near the midplane, will thus be appropriately weighted averages of this radial distribution. O. Harlen (unpublished results) has shown that the effects of such radial variations can be minimized by selecting $\Lambda_0 \approx 1$.

THE TRANSIENT EXTENSIONAL VISCOSITY Having determined the optimal aspect ratio Λ_0 of the device and determined the correct velocity profile $\dot{L}_p(t)$ to ensure ideal uniaxial kinematics in the filament, computational rheometry can be used to predict the transient extensional stress growth of a fluid sample elongated in a filament-stretching rheometer. This of course requires specification of an appropriate constitutive model for the fluid. The linear viscoelastic properties characterizing a non-Newtonian fluid can be independently determined in small amplitude oscillatory shearing (SAOS) deformations, and the nonlinear properties of some constitutive equations can be fully determined from fitting data in large amplitude deformations such as steady-shear flow or creep. The extensional stress growth can then be predicted without adjustable parameters; however, some constitutive models contain model parameters that do not affect the shear rheology and that can thus only be ascertained in extensional flows. As an example, Kolte et al. (1997) show the predicted and measured evolution in the transient extensional viscosity for a concentrated polyisobutylene solution that can be accurately described by the Papanastasiou-Scriven-Macosko (PSM) model. Filament-stretching devices thus fulfill an important rheometric role as a way of determining nonlinear fluid properties that can then be used as parameter inputs to numerical simulations of complex two-dimensional flows.

5.3. Necking and Filament Failure

Experiments in filament-stretching devices show that it is not possible to elongate a viscous or viscoelastic fluid thread to arbitrarily large Hencky strains owing to the

onset of instabilities that lead to breakup of the fluid column. Similar viscoelastic extensional instabilities have been discussed in the context of extensional rheology of polymer melts by Meissner (1985a) and are reviewed in detail by Malkin & Petrie (1997). The instabilities can arise from either the interfacial tension of the fluid or the intrinsic elasticity of the fluid column and may be conveniently subdivided into two classes: (*a*) "necking" or capillary instabilities that arise owing to the exponential growth of a surface defect $\delta R(z)$ of a given axial wavelength. The filament radius subsequently decreases to zero at a given point (typically near the axial midplane) and the filament ruptures into two topologically distinct domains; and (*b*) endplate instabilities that arise from the complex deformation field in the fluid near a rigid boundary. Such instabilities may be cohesive (i.e., occur in the fluid itself, typically owing to an interfacial fingering instability) or adhesive (i.e., occur at the interface owing to local cavitation events (Crosby et al. 2000). Because the filament profile and the magnitude of the tensile stresses that develop in viscoelastic fluids undergoing homogeneous elongation vary dramatically with both the Deborah number and the total Hencky strain accumulated, it is perhaps not surprising that each of these types of instability have been observed in filament-stretching rheometry. The three most common modes of breakup in filament stretching rheometers are detailed below.

CAPILLARY BREAKUP OF A VISCOUS THREAD For viscous Newtonian filaments undergoing elongation, the initial lubrication flow induced by the endplates ensures that the filament is always narrowest at its midplane. Using Renardy's slender-filament formulation, Hassager et al. (1998) prove that in the absence of surface tension the filament cannot fail (i.e., neck down to zero radius) in finite time. However, numerical calculations, including capillarity, indicate that the filament necks increasingly rapidly owing to the large capillary pressure in the neck (Hassager et al. 1998, Yao et al. 1998). When this local necking rate (given by Equation 15) is faster than the external scale, the motion near the midplane will be governed by a local self-similarity solution and undergo a finite time singularity. Such capillary instabilities are reviewed in detail by Eggers (1997).

ELASTIC THREAD BREAKUP AND RUPTURE Incorporating strain hardening may, at first glance, be expected to stabilize an elongating filament against capillary breakup. Such ideas are typically encapsulated in heuristic concepts such as "spinnability" of polymeric fluids (Ide & White 1976). However, although both the Oldroyd-B and Giesekus viscoelastic constitutive models are strain hardening, the evolution in the column profiles is noticeably different, as shown in Figure 8. Computations with the Oldroyd-B fluid show an increasing axial uniformity, and it becomes progressively harder to stretch the strain-hardened central region. Linear-stability analysis of the slender-filament equations (Olagunju 1999) shows that the Oldroyd-B fluid is linearly stable to perturbations for $De \geq 0.5$ even in the presence of surface tension. The addition of nonlinear terms serves to make the filament less stable in uniaxial elongation (D.O. Olagunju, unpublished work). This can be observed in the simulation with the Giesekus fluid shown in Figure 8, and the

filament, in fact, necks at a faster rate than the nonstrain-hardening Newtonian filament owing to elastic recoil near the end regions (Yao et al. 1998). Using the PSM integral model beyond a critical strain, Hassager et al. (1998) found an even more pronounced example of unstable necking. This purely elastic necking instability at very high *De* can be understood in terms of the Considère necking criterion from solid mechanics (Hart 1967, Malkin & Petrie 1997). For purely elastic fluids, the Considère criterion allowing homogeneous elongation or "spinnability" of an elastic fluid criterion can be reexpressed in terms of the familiar extensional viscosity function as

$$\left(\frac{d\ln\eta_E^+}{d\varepsilon}\right) + \left(\frac{d\ln\eta_E^+}{d\ln\dot{\varepsilon}_0}\right) \geq 1. \tag{20}$$

The extensional viscosity of polymeric fluids is typically only a very weak function of the stretch rate (or Deborah number). For such materials, spinnability is thus equivalent to requiring that the extensional viscosity increases at least exponentially with Hencky strain (McKinley & Hssager 1999). At large strains, the extensional viscosity approaches its steady-state value, the first term in Equation 20 becomes negligible, and the stability to necking perturbations requires that the extensional stress increase linearly with $\dot{\varepsilon}_0$. By contrast, reptation theories predict that the extensional stress (not the viscosity) saturate to a constant value. Entangled polymeric fluids are thus expected to be prone to necking instabilities; a situation that was anticipated by Doi & Edwards (1978).

ENDPLATE INSTABILITY AND DECOHESION Although strongly strain-hardening fluids (such as the dilute polymer solutions depicted in Figures 4 and 7) are stabilized against necking instabilities, they are prone to cohesive or adhesive instabilities near the rigid endplates. Such dynamical phenomena are important in understanding the functioning of pressure sensitive adhesives, and Crosby et al. (2000) have recently discussed the critical conditions and established useful operating diagrams for onset of different types of instability. For viscoelastic fluid samples with very small aspect ratios or for rubbery viscoelastic solid samples, it is typical to observe the onset of an adhesive instability in the form of cavitation bubbles distributed across the plate surface. The bubbles nucleate owing to the large negative (gage) pressure generated between the rigid disks, and as the plates are separated further, they evolve into strain-hardening viscoelastic fibrils (Gay & Leibler 1999). By contrast, for viscous fluids, the initial perturbations arise from the Saffman-Taylor meniscus instability and develop as a result of the unfavorable pressure gradient across the interface that results from the reverse squeeze flow. This gradient can become very large for small aspect ratios $\Lambda_0 \ll 1$; however, for larger aspect ratios, the pressure gradients are small, and Newtonian filaments remain axisymmetric near the endplates as they neck down near the midplane.

For strongly strain-hardening viscoelastic fluids, a new mode of peeling instability is observed, as shown in Figure 9*a*. The mechanism for this symmetry-breaking instability is still not definitively resolved, with both adverse pressure gradients

(a)

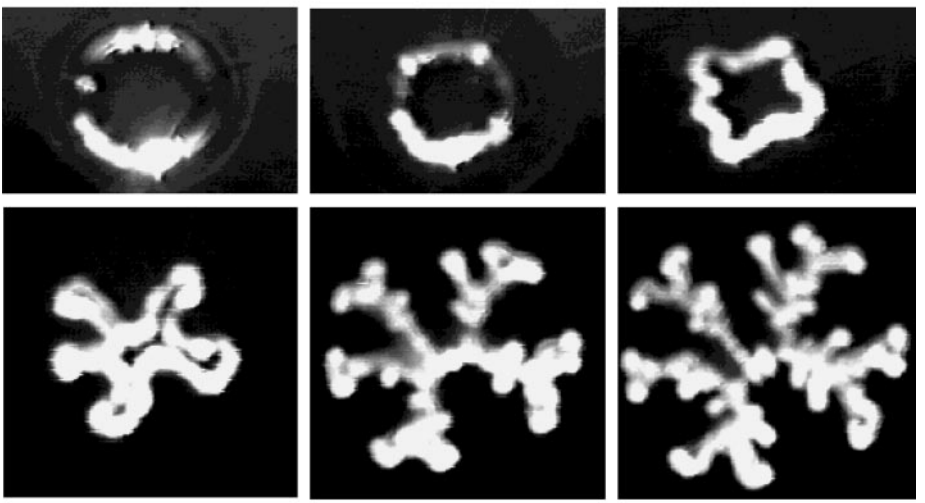

(b)

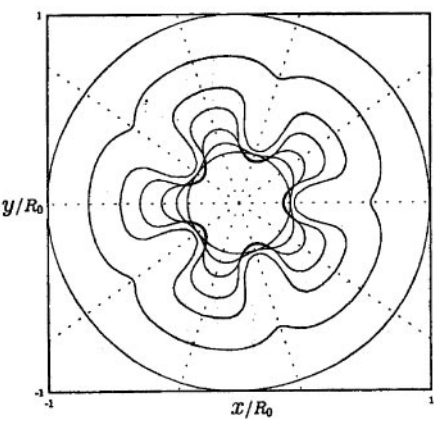

Figure 9 Endplate instability in elastic materials. (*a*) Images of the free surface of a PIB/PB Boger fluid filament elongated at $De = 2$, as viewed through a transparent glass fixture. The field of view is approximately 4 mm × 4 mm (Reproduced from Spiegelberg & McKinley 1996); (*b*) three-dimensional time-dependent simulation showing elastic endplate instability in the UCM model. Plan view showing cross sections at $z/R_0 = 0$, 0.05, 0.1, 0.2, 0.5, 1, and 12.1 at $De = 1$ and with a Hencky strain of $\varepsilon = 2.5$ (Reproduced from Rasmussen & Hassager 1998).

induced near the rigid endplate by the large tensile elastic stresses in the fluid column (Spiegelberg & McKinley 1996, Rasmussen & Hassager 1998) and compressive azimuthal stresses leading to a local buckling of the inward-flowing fluid (Arun Kumar & Graham 2000) proposed as possible driving forces. Varying the geometry of the endplates to reduce the local axial curvature of the filament can mitigate the onset of instability, and this appears to support the importance of the pressure gradients near the endplates (Gupta et al. 2000). As the filament is elongated, material is progressively withdrawn from the quasi-static fluid reservoirs (of scale R) near either endplate. Ultimately, observations (Spiegelberg & McKinley 1996) and calculations (Kolte et al. 1997) show that the free surface may locally form a "dimple" and become a nonmonotonic function of z. A time-dependent three-dimensional numerical simulation of this disturbance growth using the upper convected Maxwell (UCM) model is shown in Figure 9*b*. The absence of a solvent viscosity in these calculations means that the predicted growth rate of the perturbations is faster than observed experimentally, whereas the omission of surface tension leads to a lack of wavelength selection. More recent computations (Rasmussen & Hassager 2001) show that the most unstable wavenumber is a function of the elasto-capillary number $\phi \equiv De/Ca = \lambda\sigma/(\eta R_0)$. This dimensionless parameter is a material property that varies with the elastic modulus $G \approx \eta/\lambda$ of the fluid. As G is increased, the most unstable wavenumber of the fibrils also increases, in line with experimental measurements using commercial pressure sensitive adhesives in which $\phi \ll 1$ and the azimuthal wavenumber is very large (Ferguson et al. 1997).

6. FILAMENT STRETCHING AND MOLECULAR RHEOLOGY OF DILUTE SOLUTIONS

The numerical simulations and experimental protocols described above have shown that it is possible for filament-stretching extensional rheometers to quantitatively determine the evolution in the extensional viscosity of a viscoelastic fluid as a function of Hencky strain and Deborah number. These experimental measurements can then be compared and contrasted with molecularly based models that describe the evolution of microstructure in the fluid. The rheological character of a particular polymer/solvent pair (i.e., dilute or concentrated, unentangled or entangled) can be conveniently summarized on a concentration–molecular-weight diagram (Graessley 1980). The range of concentrations c and molecular weight M_w of the test fluids used to date in filament-stretching devices have been tabulated and are represented on a c–M_w Graessley diagram that is available online (see Appendix A, available as Supplemental Material: Follow the Supplemental Material link on the Annual Reviews homepage at http://www.annualreviews.org). The solvent used in preparing a dilute polymer solution suitable for filament stretching must be highly viscous to ensure that gravitational sagging is unimportant and that the tensile forces are measurably large. Consequently, most experiments have focused on the ideal elastic liquids known as Boger fluids (Prilutski et al. 1983).

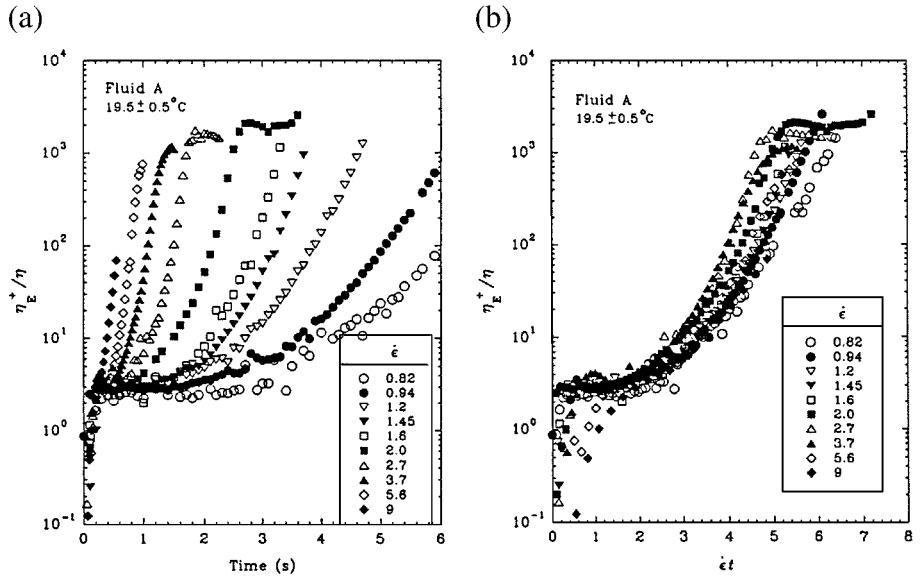

Figure 10 The transient Trouton ratio $Tr^+ = \eta_E^+/\eta_0$ for a semidilute solution of 0.31 wt% PIB in PB stretched over a range of strain rates $0.82 \leq \dot{\varepsilon}_0 \leq 9s^{-1}$ and plotted as (*a*) a function of elapsed time t and (*b*) as a function of total Hencky strain $\varepsilon = \dot{\varepsilon}_0 t$ (Reproduced from Tirtaatmadja & Sridhar 1993).

6.1. Extensional Stress Growth in Dilute Polymer Solutions

The most direct measurement to make in a filament-stretching rheometer is the time evolution in the tensile stress $\Delta\tau^+(\dot{\varepsilon}_0, t)$ during uniaxial elongation at a constant imposed deformation rate $\dot{\varepsilon}_0$. Representative results for a semidilute polyisobutylene/polybutene (PIB/PB) Boger fluid are shown in Figure 10 over a range of strain rates. When plotted as a function of time (or alternatively t/λ), the onset of strain hardening is observed at progressively earlier times as $\dot{\varepsilon}_0$ increases. However, when replotted as a function of the Hencky strain (cf. Figure 10*b*), the data approximately superimpose, and the material can rightly be referred to as a nonlinear elastic liquid because the extra stress can be simply thought of as $\Delta\tau(\dot{\varepsilon}_0, \varepsilon) \cong \eta_E^+(\varepsilon)\dot{\varepsilon}_0$ with a linear dependence on strain rate and a material coefficient that depends principally on the Hencky strain.

At short times, the data show that the Trouton ratio is small and approximately constant, and the extra stress is provided solely by the viscous Newtonian solvent. For a truly dilute polymer solution ($c < c^*$), the solvent viscosity is only $O(c)$ different from the limiting zero-shear-rate viscosity of the solution. However, as the polymer concentration increases, the initial solvent contribution diminishes in importance, and this initial plateau in the Trouton ratio decreases in relative magnitude. After an elapsed Hencky strain of $2 \leq \varepsilon \leq 3$, the polymeric contribution

to the stress exceeds that of the solvent, and the Trouton ratio climbs. Very recently, bead-spring computations by Li & Larson (2001) incorporating excluded-volume effects have shown that the precise value of the strain at which this increase in Tr^+ occurs is a very sensitive function of the excluded-volume exponent ν and, thus, of the thermodynamic quality of the solvent chosen.

The general trends in the data are in good qualitative agreement with expectations of nonlinear bead-spring kinetic theory. The extent of the strain hardening observed before the steady-state extensional viscosity is approached is of the correct order of magnitude, with a weak dependence on *De*. However, numerous researchers have shown that systematic differences appear when quantitative comparisons with the FENE-P dumbbell or the FENE-PM multibead-spring model are attempted. The parameters for these models can all be determined a priori from molecular properties of the chain and linear viscoelastic measurements of the relaxation spectrum for the fluid. Although the general trend is similar, the models consistently underpredict the stress growth at intermediate strains and predict a much more rapid transition to the final steady state. Empirical fits to the measured extensional data can readily be obtained using multimode bead-spring models in which the extensibility of each mode is selected arbitrarily (Tirtaatmadja & Sridhar 1995, Verhoef et al. 1998). However, as we show in the following sections, the molecular origins of this discrepancy have only been elucidated over the past 4 years through the careful and systematic combination of optical measurements of flow-induced birefringence, Brownian dynamics simulations of multilink chains, and single-molecule fluorescence-imaging experiments.

6.2. The Effects of Concentration and Molecular Weight

The general trends outlined above are also observed for a number of dilute and semidilute linear macromolecules [PIB, PS, polyacrylamide (PAA)] over a wide range of molecular weights and concentrations. Gupta et al. (2000b) have performed an extensive study using monodisperse polystyrene solutions and show how the transient extensional viscosity results scale with c and M_w. The final steady-state values of the scaled extensional viscosity can be represented as a function of the Deborah number, as shown in Figure 11. The steady-state extensional viscosity increases dramatically at $De \sim O(1)$ and reaches a maximum value at $De \sim 10$. At higher Deborah numbers, the steady-state extensional viscosity appears to decrease again. Such a response is expected in entangled polymer melts; reptation theories (Doi & Edwards 1986) show that the extensional stresses saturate at a constant value, and thus the Trouton ratio scales as $Tr \sim De^{-1}$. Simple dumbbell theories for dilute solutions give $Tr \sim De^0$; however, more complex constitutive models that incorporate configuration-dependent drag on the chain (arising from the constraining effects of other nearby chains, for example) can show a maximum in the extensional viscosity (Bird & Wiest 1995). Asymptotic analysis of the Wiest model suggests $Tr \sim De^{-1/2}$ is in good agreement with the experimental data (Gupta et al. 2000b). The results in Figure 11 thus indicate that

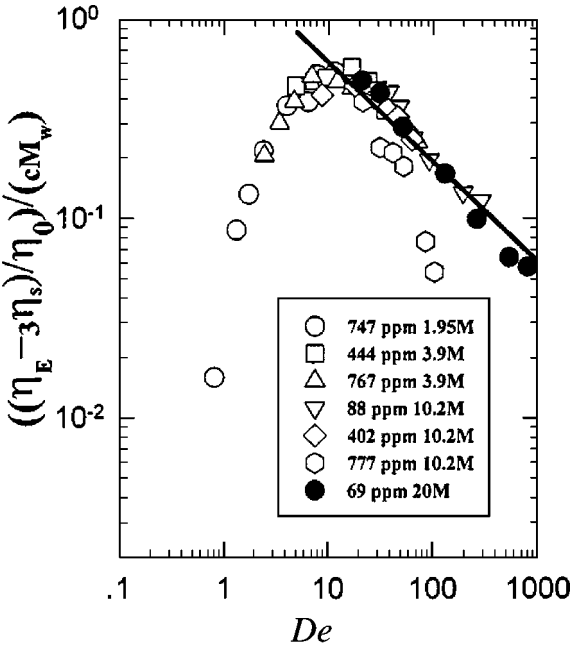

Figure 11 The variation in the steady-state extensional viscosity with increasing Deborah number for a series of high molecular-weight dilute polystyrene solutions. The line shows the asymptotic prediction of the Wiest model (Reproduced from Gupta et al. 2000b).

accurately modeling hydrodynamic interactions (both intra- and interchain) is very important in strong elongational flows.

6.3. Stress Relaxation and Molecular Hysteresis

As we have indicated in Section 4.2, extensional stress relaxation following the cessation of stretching at time t_1 can also be measured in a filament-stretching rheometer. After the endplates are stopped at a predetermined maximum strain ε_1, the force rapidly decays. However, because $\rho g L(t_1)/\Delta\tau_p(t_1) \ll 1$ and $(\sigma/R_{mid}(t_1))/\Delta\tau_p(t_1) \ll 1$, the large elastic stresses in the elongated filament retard the onset of both gravitational sagging and capillary-induced drainage. The tensile force and column radius can thus be used to compute the tensile-stress relaxation function $\Delta\tau^-(\dot{\varepsilon}_0, (t - t_1))$, where $\dot{\varepsilon}_0$ is the imposed stretch rate during the previous extension. Experiments show this relaxation is much faster than that measured following cessation of steady-shear flow at a kinematically equivalent steady shear rate of $\dot{\gamma}_0 = \sqrt{3}\dot{\varepsilon}_0$ (Spiegelberg & McKinley 1996, Orr & Sridhar 1996). The rapid decrease in the stress following uniaxial elongation arises from the nonlinearity in the elastic-spring law for the chain when it is near full extension. The

increased stiffness in the spring reduces the effective relaxation time to $\gamma_1/f(tr\boldsymbol{A})$, and asymptotic analysis of the FENE-P dumbbell equation shows that, although the polymeric stretch $tr\boldsymbol{A}$ relaxes exponentially with this effective time constant, the polymeric stress in fact decreases as $(t-t_1)^{-1/2}$ (Doyle et al. 1998). Brownian dynamics simulations of bead-rod chains support this conclusion and show that the stress may reduce by a factor of 50 in an elapsed time as small as $\Delta t \sim 0.5\lambda$. The simulations and asymptotic analysis show that the relaxation curves measured following elongation to steady state at different stretch rates are, in fact, all part of a universal function and can all be superimposed on a single master curve by the application of a single additive shift factor in time given by $t_r = (t-t_1) + a_\varepsilon$, with $a_\varepsilon = 1/(8De^2)$ (Doyle et al. 1998).

The consequences of these differences in the evolution in the polymeric conformation (or end-to-end length of the chain) and the resulting stress in the chain during stretching and relaxation are manifested macroscopically as a *stress-conformation hysteresis*. Fiber-spinning experiments (Talbott & Goddard 1979) had previously shown that the stress-optical rule (see Equation 7) becomes invalid in strong extensional flows of polymer solutions. However, the flow in a spin line is a steady Eulerian flow, and what had not been observed to date is that in a strong transient flow the coefficient C, in fact, becomes a functional of the full deformation history. This has now been demonstrated both experimentally and numerically in unsteady flows with either uniaxial or planar kinematics (Doyle et al. 1998, Kwan & Shaqfeh 1998). The dimensionless anisotropy in the molecular conformation ΔA can still be determined optically by measuring the flow-induced birefringence (Wiest 1995). Assuming that, on the level of a single spring, the local segments have a Gaussian distribution leads to the following expression for the conformation

$$\frac{\langle Q_z Q_z \rangle - \langle Q_r Q_r \rangle}{(Nb^2/3)} = \Delta A(t) = \frac{\Delta n'(t)}{C \nu k_B T}, \tag{21}$$

where C is the usual stress-optical coefficient and the equilibrium coil size of the bead-spring chain is $R_g^2 = Nb^2$. The stress-optical rule does not need to be invoked because the evolution in the actual polymeric stress in the filament is independently measured using the mechanical force transducer. Experimental and numerical results for several dilute solutions of polystyrene are shown in Figure 12. During transient uniaxial elongation (*upper curves*), the total stress increases much more rapidly than the Hookean or linear-elastic contribution to the stress $\Delta\tau_e = \nu k_B T \Delta A$. When stretching stops, the total stress drops much more rapidly than the birefringence (*lower curves*).

6.4. Modeling of Stress-Conformational Hysteresis

Stress-conformation hysteresis is completely absent in simple closed-form viscoelastic constitutive equations such as the Oldroyd-B, FENE-P dumbbell, or FENE-PM bead-spring chain models. It is, however, captured by numerical calculations with more realistic models having additional internal degrees of freedom

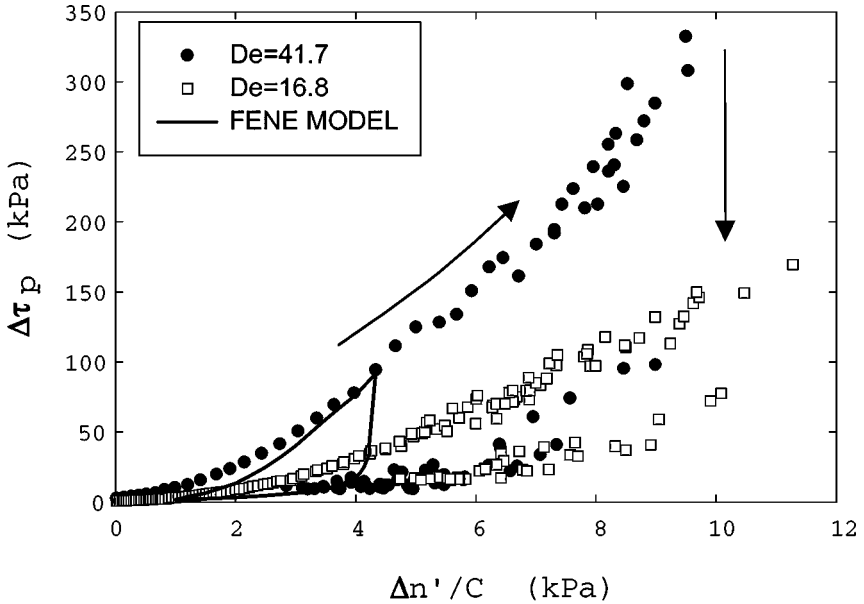

Figure 12 Experimental measurements and numerical simulations of stress-conformation hysteresis in dilute polystrene solutions during rapid elongation (Reproduced from Sridhar 2000).

such as FENE dumbbell ensembles, FENE-P chains, and Brownian dynamics simulations of bead-rod or bead-spring chains. The area contained within the hysteresis loops corresponds to additional mechanical energy that is dissipated during a strong unsteady flow and that is not recovered elastically; a situation that was first considered by Ryskin (1987). On a macroscopic level, this extra dissipation may assist in helping to rationalize systematic differences between computation and experiment that have been observed in prototypical complex flows such as settling of a sphere through an elastic liquid or the flow through an axisymmetric contraction (Rothstein & McKinley 2001). On a microscopic level, this hysteretic behavior is now known to have at least two sources (Ghosh et al. 2001) as outlined below:

CONFIGURATIONAL HYSTERESIS Brownian dynamics show that the set of configurations experienced by a single bead-rod or bead-spring chain are very different during stretching or relaxation. This is shown in the chain configurations of Figure 13*a*. For a given end-to-end length, the total stress associated with highly kinked and locally stretched configurations such as the "yo-yo" is much higher than that associated with the uniformly "crumpled" and partially relaxed chain configurations observed during relaxation (Doyle et al. 1998).

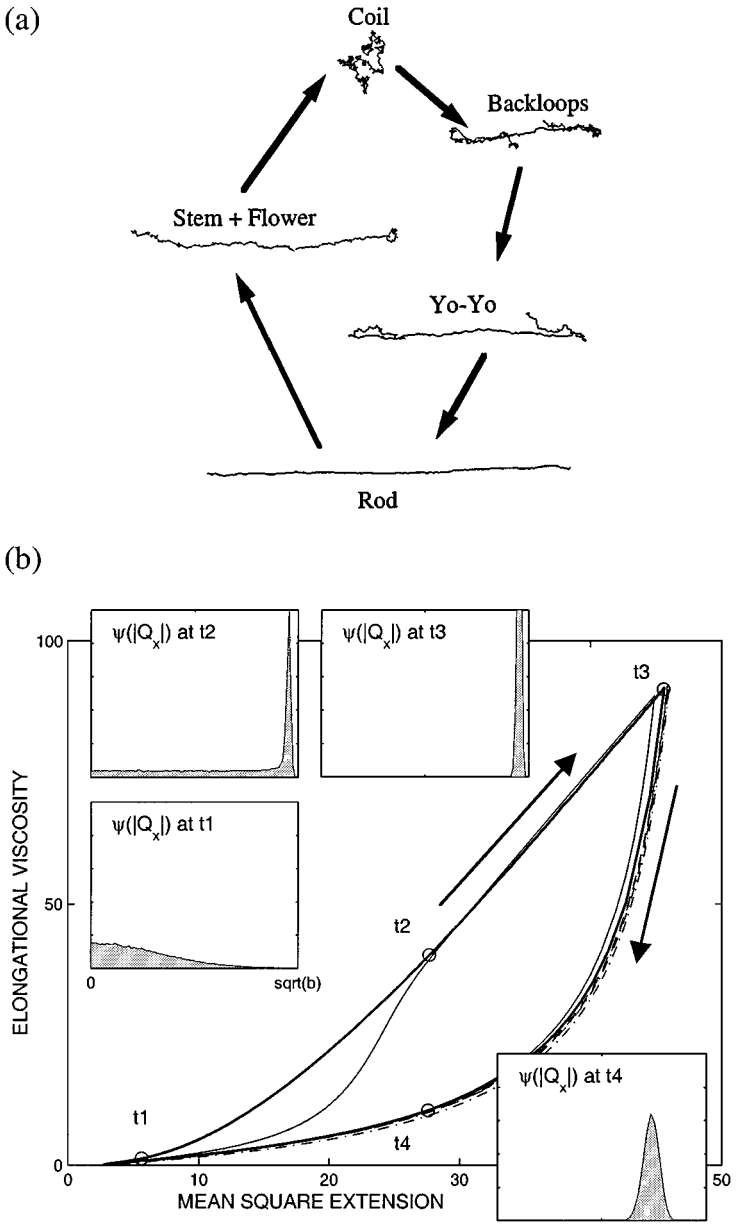

Figure 13 Molecular hysteresis during rapid uniaxial elongation. (*a*) Conformational hysteresis: a series of snapshots showing some characteristic conformational states observed during a Brownian-dynamics simulation of the unraveling and subsequent relaxation of a 200-link bead-rod chain at $De = 11.4$ (Reproduced from Doyle et al. 1998). (*b*) Distributional hysteresis: transient uniaxial elongation and subsequent relaxation of an ensemble of 5000 FENE dumbbells with extensibility parameter $L^2 = 50$ at $De = 6.0$. The insets show the probability density ψ of finding a dumbbell with a given value of $|Q_x|$ at the indicated times, t1, t2, t3, t4 (Reproduced from Sizaire et al. 1999).

DISTRIBUTIONAL HYSTERESIS On a macroscopic level, the total stress or birefringence measured experimentally is derived from an ensemble of polymer dumbbells or chains. In simple models such as the FENE-P dumbbell, this distribution is assumed to be initially Gaussian and remains a (skewed) Gaussian at all future times. Brownian-dynamics calculations during transient elongation, however, show this not to be true (Keunings 1997, Sizaire et al. 1999). Samples of the probability density distribution of the dumbbell length $\psi(|Q_x|, t)$ projected in the stretching direction are shown as insets to the curve of extensional viscosity vs. mean square extension in Figure 13*b*. Even though the polymer chain is modeled as a dumbbell, with no internal structure, the non-Gaussian distribution of dumbbells during rapid stretching leads to hysteretic behavior. The shape of this curve looks very similar to that observed in experiments.

The physical origin of both these sources of hysteresis is the rapid and transient nature of the stretching process. When the timescale for stretching ($\dot{\varepsilon}_0^{-1}$) exceeds the natural timescale of the molecule, then it can no longer be assumed that the chain has time to sample its entire conformational phase space, i.e., the stretching is no longer a quasi-equilibrium thermodynamic process, and the usual bead-spring force-extension curve is no longer valid during stretching (Ghosh et al. 2001). It is for this reason that the measured tensile force lies above that predicted by simple dumbbell models. As stretching proceeds and the chain approaches full elongation, the total extent of the configurational phase space available contracts and once again the stress in the chain is well described by a simple FENE-P dumbbell theory (Doyle et al. 1998).

As a result of the rapid and nonequilibrium nature of the transient elongation, the initial configuration of every molecule and the distribution of these configurations then becomes important; a process coined "molecular individualism" (de Gennes 1997). Using fluorescently labeled DNA molecules that are large enough to be imaged individually, Chu and co-workers documented this process in a series of seminal publications (see, for example, Smith & Chu 1998, Perkins et al. 1999). A representative set of images and equivalent Brownian dynamics configurations are shown in Figure 14 for a true molecular dumbbell configuration. Such simulations faithfully capture both the unraveling process of individual chains and the evolution in the distributions of different characteristic configurations such as "loops," "folds," and "dumbbells" (Larson et al. 1999). The source of heterogeneity in the flow-induced configurations observed at high *De* is caused by the distribution of initial chain configurations.

When the number of repeat units in the simulated chain is rescaled to match that of longer and more flexible polystyrene solutions and the force-extension law is changed from that of the worm-like chain (appropriate to DNA chains) to that of a flexible polymer chain (i.e., the FENE spring), excellent agreement with experimental measurements of the evolution in the tensile stress is obtained. To demonstrate this, we show in Figure 15 a comparison between numerical computations with a bead-spring ($M = 20$) chain and the experimentally measured stress growth and the subsequent stress relaxation following cessation of stretching

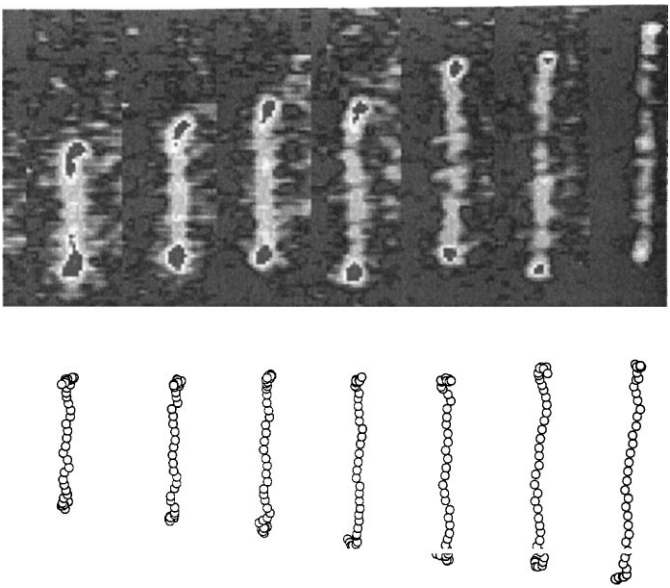

Figure 14 Individual molecular conformations of fluoroescently labeled DNA molecules during rapid planar elongation and equivalent realizations of a 20-link bead-rod chain (Reproduced from Larson et al. 1999).

(Li et al. 2000). All of the model parameters are determined from the primary molecular structure of the chain or from linear viscoelastic experiments, and the agreement is very satisfying, provided the thermodynamic quality of the solvent is correctly accounted for (Li & Larson 2001). Some discrepancies remain in the rapid nonlinear stress relaxation at long times. As the molecular weight or Deborah number is increased to very large values ($De \geq 30$), the agreement becomes less satisfactory, most likely owing to additional effects of hydrodynamic interaction of the polymer chains with the solvent that are not incorporated in the basic bead-spring chain model (cf. Section 6.2).

Simulation of complex viscoelastic flows using bead-rod chain or bead-spring chain models with so many internal degrees of freedom is still not computationally feasible, and much recent work has been directed at developing simpler, closed-form models that accurately capture or "coarse-grain" the macroscopic stress-conformation hysteresis arising from molecular individualism on the microscale. The first models treated the additional stress arising from the strong local rate of deformation as explicitly viscous-like (see for example Rallison 1997, Verhoef et al. 1998), whereas more recent models have attempted to capture the progressive changes in the average internal structure of the molecules during stretching and relaxation using additional scalar evolution equations (Lielens et al. 1998, Lhuillier 2001). It remains to be seen which approach best describes kinematically

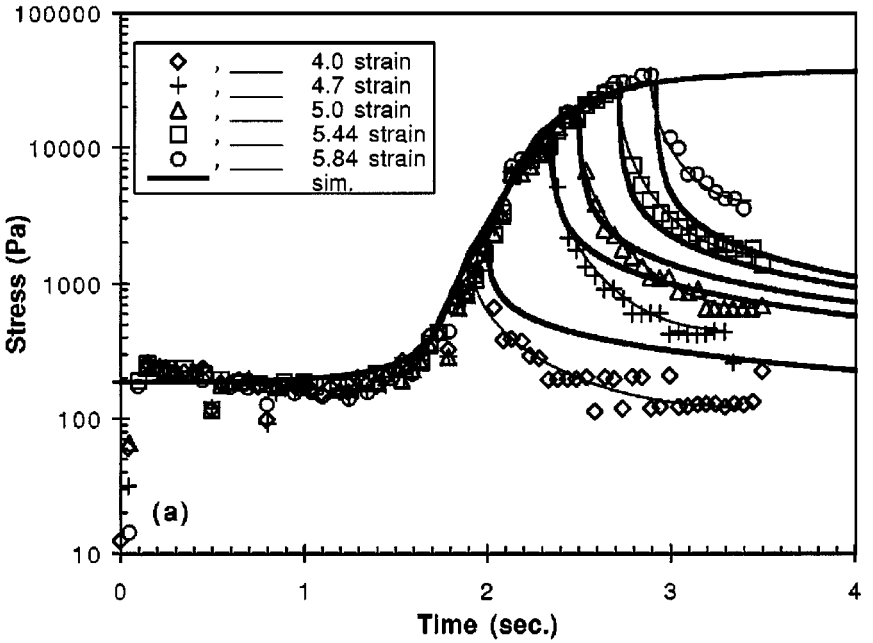

Figure 15 Comparison of the transient Trouton ratio measured in a dilute polystyrene solution ($c = 88$ ppm, $M_w = 10.2 \times 10^6$ g/mol) with predictions of a 20-bead-spring chain model (Reproduced from Li et al. 2000).

complex "mixed" flows of polymer solutions containing regions of both strong elongation and shearing.

6.5. Other Complex Fluid Systems

Filament-stretching devices may also be able to provide corresponding levels of insight to other classes of complex fluids. As an example, we mention here semidilute and concentrated entangled polymer solutions. Although the linear viscoelastic and nonlinear shearing properties of such fluids have been extensively explored (Doi & Edwards 1986), there have been fewer quantitative investigations of strong extensional flows (Leal & Oberhauser 2000). As a consequence of the two distinct timescales discussed in Section 3.3, there are three important regimes in the steady extensional viscosity of entangled fluids, as shown in Figure 16. For low Deborah numbers, $\lambda_d \dot{\varepsilon}_0 < 1/2$, a Trouton ratio of $Tr = 3$ is expected and observed. For Deborah numbers $1/2 < \lambda_d \dot{\varepsilon}_0 < 3M_w/M_e$, the tubes constraining the entangled chains are oriented. However, on the timescale of the chain, the flow is weak (i.e., $\lambda_R \dot{\varepsilon}_0 < 1/2$), and hence, the chains relax inside their tubes and the steady extensional viscosity in fact decreases below $Tr = 3$. For even larger deformation rates, $3M_w/M_e < \lambda_d \dot{\varepsilon}_0$ (corresponding to $\lambda_R \dot{\varepsilon}_0 > 1$), chain stretching and strain

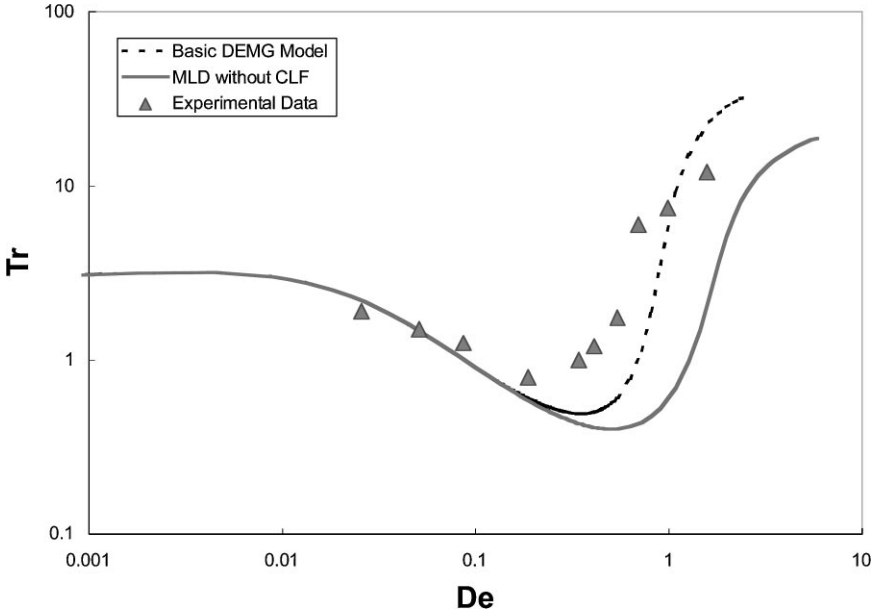

Figure 16 The steady extensional viscosity of a concentrated polystyrene solution (6.0 wt.%, $M_w = 10.2 \times 10^6$ g/mol) with $Z \approx 26$ entanglements per molecule and the associated prediction of the Doi-Edwards-Marrucci-Grizutti (DEMG) model and the Mead-Larson-Doi (MLD) model (Reproduced from P.K. Bhattacharjee, J. Oberhauser, G.H. McKinley, L.G. Leal, & T. Sridhar, submitted).

hardening in the extensional viscosity is observed. As indicated in Figure 16, the experimental measurements are in good agreement with predictions of simple differential constitutive models for entangled polymer solutions. This crossover—from extension thinning to extension thickening—also leads to an exchange in the observed mode of elastic instability, from elasto-capillary necking to fibrillar peeling instability at the endplate when $\lambda_R \dot{\varepsilon}_0 \approx 1$.

Filament-stretching tests have also been made on other complex fluid systems including liquid crystal polymer solutions (Ooi & Sridhar 1994), associative polymer solutions (McKinley 2000), and entangled star polymer solutions (X. Yee & T. Sridhar, submitted). However, space precludes further discussion of the results.

7. OUTLOOK

In the present article, we attempt to provide an overview of the kinematic considerations that must be incorporated in designing filament-stretching rheometers, the dynamics of the resulting motion for non-Newtonian fluids exhibiting strain hardening, and finally, what extensional rheometry measurements have been able

to teach us about the physics of rapid deformations in dilute polymer solutions as well as the constitutive equations we use to model such flows. The filament-stretching device has matured into a reliable method of measuring the rheological response of mobile liquids to a nearly ideal extensional deformation. The kinematics of the flow effectively isolate extensional effects from those of shearing, and it is hoped that this technique will lead to increased reporting of extensional rheological properties alongside the now standard viscometric data.

Much work remains to be done in understanding the fluid dynamics of the viscoelastic free-surface instabilities that ultimately lead to filament failure at large strains; however, additional information about the extensional rheology of the material is encoded in these responses and deserves detailed analysis. Future advances in this area will no doubt result from the same elements that have benefited the development of filament-stretching rheometry to date, i.e., a strong interplay between careful experimentation, numerical simulation, kinetic theory, and constitutive modeling.

The industrial applications of filament-stretching rheometry have only just begun to be recognized. As we note in the Introduction, extensional flow can have a dominant influence on numerous industrial processes and applications involving rheologically complex fluids including foodstuff, adhesives, and other consumer products. It is thus expected that filament-stretching rheometers will be useful both in developing new materials and in systematically investigating the effect of additives in currently used materials.

ACKNOWLEDGMENTS

The authors would like to acknowledge numerous conversations over the years with O. Hassager, M. Yao, V. Entov, O. Harlen, D.F. James, and S.J. Muller, D.A. Nguyen, E.J. Hinch, J.M. Rallison. In addition, we express our thanks to the numerous former and present students and colleagues in both laboratories who have developed many of the techniques and devices discussed in this review. Support for research in extensional rheology at M.I.T. has been provided by the National Science Foundation, the Lord Foundation, and the National Aeronautics and Space Administration. Support for research in extensional rheology at Monash has been provided by the Australian Research Council.

Visit the Annual Reviews home page at www.AnnualReviews.org

LITERATURE CITED

Anna SL, McKinley GH, Nguyen DA, Sridhar T, Muller SJ, et al. 2001. An inter-laboratory comparison of measurements from filament-stretching rheometers using common test fluids. *J. Rheol.* 45:83–14

Anna SL, Rogers CB, McKinley GH. 1999. On controlling the kinematics of a filament stretching rheometer using a real-time active control mechanism. *J. Non-Newton. Fluid. Mech.* 87:307–35

Arun Kumar K, Graham MD. 2000. Buckling instabilities in models of viscoelastic free-surface flows. *J. Non-Newton. Fluid Mech.* 89:337–51

Astarita G, Nicodemo L. 1970. Extensional flow behavior of polymer solutions. *Chem. Eng. J.* 1:57–66

Baaijens FPT. 1998. Mixed finite element methods for viscoelastic flow analysis: a review. *J. Non-Newton. Fluid Mech.* 79(2–3):361–85

Bazilevsky AV, Entov VM, Rozhkov AN. 1990. In *Third European Rheology Conference*, ed. DR Oliver, pp. 41–43. Amsterdam: Elsevier

Bird RB. 1982. Polymer kinetic theories and elongational flows. *Chem. Eng. Commun.* 16:175–87

Bird RB, Armstrong RC, Hassager O. 1987a. *Dynamics of Polymeric Liquids*. Volume 1: *Fluid Mechanics*. New York: Wiley Intersci.

Bird RB, Curtiss CF, Armstrong RC, Hassager O. 1987b. *Dynamics of Polymeric Liquids*. Volume 2: *Kinetic Theory*. New York: Wiley Intersci.

Bird RB, Wiest JM. 1995. Constitutive equations for polymeric liquids. *Annu. Rev. Fluid Mech.* 27:169–93

Brandrup H, Immergut EH. 1997. *Polymer Handbook*. New York: Wiley

Crosby AJ, Shull KR, Lakrout H, Creton C. 2000. Deformation and failure modes of adhesively bonded elastic layers. *J. Appl. Phys.* 88:2956–66

de Gennes P-G. 1974. Coil-stretch transition of dilute flexible polymers under ultra-high velocity gradients. *J. Chem. Phys.* 60:5030–42

de Gennes P-G. 1997. Molecular individualism. *Science* 276:1999

Doi M, Edwards SF. 1978. Dynamics of concentrated polymer systems. IV. Rheological properties. *J. Chem. Soc. Faraday Trans. II* 75:38–54

Doi M, Edwards SF. 1986. *The Theory of Polymer Dynamics*. Oxford: Oxford Univ. Press

Dontula P, Pasquali M, Scriven LE, Macosko CW. 1997. Can extensional viscosity be measured with opposed-nozzle devices. *Rheol. Acta* 36:429–48

Doyle P, Shaqfeh ESG, McKinley GH, Spiegelberg SH. 1998. Relaxation of dilute polymer solutions following extensional flow. *J. Non-Newton. Fluid Mech.* 76(1–3):79–110

Eggers J. 1997. Nonlinear dynamics and breakup of free-surface flows. *Rev. Mod. Phys.* 69(3):865–929

Entov VM, Kordonskil VI, Prokhorov IV, Rozhkov AN, Toropov AI, et al. 1988. Rapid stretching of polymer solutions. *Sov. Phys. Dokl.* 33(8):628–30

Ferguson J, Reilly B, Granville N. 1997. Extensional and adhesion characteristics of a pressure sensitive adhesive. *Polymer* 38(4):795–800

Fuller GG. 1995. *Optical Rheometry of Complex Fluids*. Oxford: Oxford Univ. Press

Fuller GG, Cathey CA, Hubbard B, Zebrowski BE. 1987. Extensional viscosity measurements for low viscosity fluids. *J. Rheol.* 31(3):235–49

Gaudet S, McKinley GH. 1998. Extensional deformation of non-Newtonian liquid bridges. *Comput. Mech.* 21:461–76

Gay C, Leibler L. 1999. On stickiness. *Phys. Today* 82:48–52

Ghosh I, McKinley GH, Brown RA, Armstrong RC. 2001. Deficiencies of FENE dumbbell models in describing the rapid stretching of dilute polymer solutions. *J. Rheol.* 45:721–58

Graessley WW. 1980. Polymer chain dimensions and the dependence of viscoelastic properties on concentration, molecular weight and solvent power. *Polymer* 21:258–62

Gupta RK, Nguyen DA, Sridhar T. 2000. In *Proc. 13th Int. Congr. Rheol.*, ed. DM Binding, NE Hudson, J Mewis, J-M Piau, CJS Petrie, et al. 3:203–5. Cambridge, UK: Br. Soc. Rheol.

Gupta RK, Nguyen DA, Sridhar T. 2000. Extensional viscosity of dilute polystyrene solutions—effect of concentration and molecular weight. *Phys. Fluids* 12(6):1296–318

Gupta RK, Sridhar T. 1998. In *Rheological Measurement*, ed. AA Collyer, DW Clegg, pp. 211–45. London: Elsevier Appl. Sci. 2nd ed.

Hart EW. 1967. Theory of the Tensile Test. *Acta Metall.* 15:351–55

Hassager O, Kolte MI, Renardy M. 1998. Failure and nonfailure of fluid filaments in extension. *J. Non-Newton. Fluid Mech.* 76(1–3): 137–52

Ide Y, White JL. 1976. The spinnability of polymer fluid filaments. *J. Appl. Polym. Sci.* 20:2511–31

James DF, Walters KA. 1993. In *Techniques in Rheological Measurement*, ed. AA Collyer, pp. 33–53. London: Elsevier

Keunings R. 1997. On the Peterlin approximation for finitely extensible dumbbells. *J. Non-Newton. Fluid Mech.* 68:85–100

Kolte MI, Rasmussen HK, Hassager O. 1997. Transient filament stretching rheometer. II: Numerical simulation. *Rheol. Acta* 36:285–302

Kwan TCB, Shaqfeh ESG. 1998. Brownian dynamics simulations of the stress and molecular configuration of polymers in exponential and linearly-ramped shear flow. *J. Non-Newton. Fluid Mech.* 82(2-3):139–65

Larson RG. 1988. *Constitutive Equations for Polymer Melts and Solutions*. Boston: Butterworths

Larson RG, Hua H, Smith DE, Chu S. 1998. Brownian dynamics simulations of a DNA molecule in an extensional flow field. *J. Rheol.* 43:267–304

Leal LG, Oberhauser JP. 2000. Non-Newtonian fluid mechanics for polymeric liquids: a status report. *Korea-Aust. J. Rheol.* 12:1–26

Lhuillier D. 2001. A possible alternative to the FENE dumbbell model of dilute polymer solutions. *J. Non-Newton. Fluid Mech.* 97:87–96

Li J-M, Burghardt WR, Yang B, Khomami B. 1998. Flow birefringence and computational studies of a shear-thinning polymer solution in axisymmetric stagnation flows. *J. Non-Newton. Fluid Mech.* 74(1–3):151–94

Li L, Larson RG. 2001. Excluded volume effects on the birefringence and stress of dilute polymer solutions in extensional flow. *Rheol. Acta* 39(5):419–27

Li L, Larson RG, Sridhar T. 2000. Brownian dynamics simulations of dilute polystyrene solutions. *J. Rheol.* 44(2):291–323

Lielens G, Halin P, Jaumain I, Keunings R, Legat V. 1998. New closure approximations for the kinetic theory of finitely extensible dumbbells. *J. Non-Newton. Fluid Mech.* 76:249–80

Malkin AY, Petrie CJS. 1997. Some conditions for rupture of polymeric liquids in extension. *J. Rheol.* 41(1):1–25

Matta JE, Tytus RP. 1990. Liquid stretching using a falling cylinder. *J. Non-Newton. Fluid Mech.* 35:215–29

McKinley GH. 2000. In *Proc. 13th Int. Congr. Rheol.*, ed. DM Binding, NE Hudson, J Mewis, J-M Piau, CJS Petrie, et al. 1:15–22. Cambridge, UK: Br. Soc. Rheol.

McKinley GH, Brauner O, Yao M. 2001. Kinematics of filament stretching in dilute and concentrated polymer solutions. *Korea-Aust. J. Rheol.* 13:29–35

McKinley GH, Hassager O. 1999. The considère condition and rapid stretching of linear and branched polymer melts. *J. Rheol.* 43(5):1195–212

Mead DW, Larson RG, Doi M. 1998. A molecular theory for fast flows of entangled polymers. *Macromolecules* 31:7895–914

Meissner J. 1985a. Experimental aspects in polymer melt elongational rheology. *Chem. Eng. Commun.* 33:159–80

Meissner J. 1985b. Rheometry of polymer melts. *Annu. Rev. Fluid Mech.* 17:45–64

Münstedt H. 1979. New universal extensional rheometer for polymer melts. Measurements on a polystyrene sample. *J. Rheol.* 24(6):847–67

Nguyen TQ, Kausch H-H, eds. 1999. *Flexible Polymer Chain Dynamics in Elongational Flow*. Berlin: Springer-Verlag

Nitschmann H, Schrade J. 1948. On the fibreforming ability of non-Newtonian liquids. *Helv. Acta* 31:297–319

Olagunju DO. 1999. A 1-D theory for extensional deformation of a viscoelastic filament under exponential stretching. *J. Non-Newton. Fluid Mech.* 87(1):27–46

Oliver DR, Bragg R. 1974. The triple jet: a

new method for measurement of extensional viscosity. *Rheol. Acta* 13:830–35

Ooi YW, Sridhar T. 1994. Uniaxial extension of a lyotropic liquid crystalline polymer solution. *Ind. Eng. Chem. Res.* 33:2368–73

Orr NV, Sridhar T. 1996. Stress relaxation in uniaxial extension. *J. Non-Newton. Fluid Mech.* 67:77–104

Orr NV, Sridhar T. 1999. Probing the dynamics of polymer solutions in extensional flow using step strain rate experiments. *J. Non-Newton. Fluid Mech.* 82:203–22

Perkins TT, Smith DE, Chu S. 1997. Single polymer dynamics in an elongational flow. *Science* 276:2016–21

Petrie CJS. 1979. *Elongational Flows: Aspects of the Behavior of Model Elasticoviscous Fluids*. London: Pitman

Petrie CJS. 1995. Extensional flow—a mathematical perspective. *Rheol. Acta* 34:12–26

Phan-Thien N, Tanner RI. 1984. Lubrication squeeze-film theory for the Oldroyd-B fluid. *J. Non-Newton. Fluid Mech.* 14:327–35

Prilutski G, Gupta RK, Sridhar T, Ryan ME. 1983. Model viscoelastic liquids. *J. Non-Newton. Fluid Mech.* 12:233–41

Rallison JM. 1997. Dissipative stresses in dilute polymer solutions. *J. Non-Newton. Fluid Mech.* 68:61–83

Rasmussen HK, Hassager O. 1998. Three-dimensional simulations of viscoelastic instability in polymeric filaments. *J. Non-Newton. Fluid Mech.* 82:189–202

Rasmussen HK, Hassager O. 2001. The role of surface tension on the elastic decohesion of polymeric filaments. *J. Rheol.* 45:527–37

Renardy M. 1994. Some comments on the surface-tension driven breakup (or the lack of it) of viscoelastic jets. *J. Non-Newton. Fluid Mech.* 51:97–107

Rothstein JP, McKinley GH. 2001. The axisymmetric contraction-expansion: the role of extensional rheology on vortex growth dynamics and the enhanced pressure drop. *J. Non-Newton. Fluid Mech.* 98:33–63

Ryskin G. 1987. Calculation of the effect of polymer additive in a converging flow. *J. Fluid Mech.* 178:423–40

Schultz WW. 1982. One-dimensional liquid fibers. *J. Rheol.* 26(4):331–45

Shipman RWG, Denn MM, Keunings R. 1991. Mechanics of the 'falling plate' extensional rheometer. *J. Non-Newton. Fluid Mech.* 40:281–88

Sizaire R, Legat V. 1997. Finite element simulation of a filament stretching extensional rheometer. *J. Non-Newton. Fluid Mech.* 71(1–2):89–108

Sizaire R, Lielens G, Jaumain I, Keunings R, Legat V. 1999. On the hysteretic behavior of dilute polymer solutions in relaxation following extensional flow. *J. Non-Newton. Fluid Mech.* 82(2–3):233–54

Smith DE, Chu S. 1998. The response of flexible polymer coils to a sudden high strain rate flow. *Science* 281:1335–40

Solomon MJ, Muller SJ. 1996. The transient extensional behavior of polystyrene-based boger fluids of varying solvent quality and molecular weight. *J. Rheol.* 40(5):837–56

Spiegelberg SH, Ables DC, McKinley GH. 1996. The role of end-effects on measurements of extensional viscosity in viscoelastic polymer solutions with a filament stretching rheometer. *J. Non-Newton. Fluid Mech.* 64(2–3):229–67

Spiegelberg SH, McKinley GH. 1996. Stress relaxation and elastic decohesion of viscoelastic polymer solutions in extensional flow. *J. Non-Newton. Fluid Mech.* 67:49–76

Sridhar T. 1990. An overview of the Project M1. *J. Non-Newton. Fluid Mech.* 35:85–92

Sridhar T. 2000. From rheometry to rheology. *Korea-Aust J. Rheol.* 12:39–53

Sridhar T, Nguyen DA, Fuller GG. 2000. Birefringence and stress growth in uniaxial extension of polymer solutions. *J. Non-Newton. Fluid Mech.* 90(2–3):299–315

Sridhar T, Tirtaatmadja V, Nguyen DA, Gupta RK. 1991. Measurement of extensional viscosity of polymer solutions. *J. Non-Newton. Fluid Mech.* 40:271–80

Szabo P. 1997. Transient filament stretching rheometer. I: force balance analysis. *Rheol. Acta* 36:277–84

Talbott WH, Goddard JD. 1979. Streaming birefringence in extensional flow of polymer solutions. *Rheol. Acta* 18:505–17

Tanner RI. 2000. *Engineering Rheology*. Oxford: Clarendon

Tirtaatmadja V, Sridhar T. 1993. A filament stretching device for measurement of extensional viscosity. *J. Rheol.* 37:1081–102

Tirtaatmadja V, Sridhar T. 1995. Comparison of constitutive equations for polymer solutions in uniaxial extension. *J. Rheol.* 39(6):1133–60

Trouton FT. 1906. On the coefficient of viscous traction and its relation to that of viscosity. *Proc. R. Soc. London Ser. A* 77:426–40

van den Brule BHAA. 1993. Brownian dynamics simulation of finitely extensible bead-spring chains. *J. Non-Newton. Fluid Mech.* 47:357–78

Verhoef MRJ, van den Brule BHAA, Hulsen MA. 1998. On the modelling of a PIB/PB Boger fluid in extensional flow. *J. Non-Newton. Fluid Mech.* 80(2–3):155–82

Watanabe H. 1999. Viscoelasticity and dynamics of entangled polymers. *Prog. Polym. Sci.* 24:1253–403

Wiest JM. 1999. Birefringence in strong flows of polymer solutions. *Polymer* 40:1917–22

Yao M, McKinley GH. 1998. Numerical simulation of extensional deformations of viscoelastic liquid bridges in filament stretching devices. *J. Non-Newton. Fluid Mech.* 74(1–3):47–88

Yao M, McKinley GH, Debbaut B. 1998. Extensional deformation, stress relaxation and necking failure of viscoelastic filaments. *J. Non-Newton. Fluid Mech.* 79:469–501. (Special Issue dedicated to 60th birthday of M. Crochet)

Yao M, Spiegelberg SH, McKinley GH. 2000. Fluid dynamics of weakly strain-hardening fluids in filament stretching devices. *J. Non-Newton. Fluid Mech.* 89:1–43

Yildirim OE, Basaran OA. 2001. Deformation and breakup of stretching bridges of Newtonian and shear-thinning liquids: comparison of one and two-dimensional models. *Chem. Eng. Sci.* 56:211–33